Chapter One
Introduction

1.1 Introduction

There has been a rapid increase in interest in nanotechnology and the use of nanoparticles in commercial applications. However, there is little known of the fate and behavior of engineered nanoparticles in the environment. The properties of nanoparticles differ remarkably from small molecules and their chemistry and synthesis necessitates that they be considered more like complex mixtures than small molecules. The ability of the molecules to attach to the surface of nanoparticles and exchange with other molecules already placed there indicates that careful consideration of the chemistry of nanoparticles and how it relates to their fate in surface waters and sediments is key to predicting their final fate. We have set out to briefly introduce at a basic level the properties and synthesis of nanoparticles and then review the state of current understanding relating to the fate and behavior of nanoparticles in the environments with particular focus on engineered nanoparticles [1].

Nanoparticles and their origins Nanoparticles are generally defined as particulate matter with at least one dimension that is less than 100 nm. This

definition puts them in a similar size domain as that of ultrafine particles (air borne particulates) and places them as a sub-set of colloidal particles. A considerable fraction of the solid matter on earth can

be found in the size range of colloids and nanoparticles. In the last 2 decades' scientists have shown that colloids and nanoparticles are present everywhere in the environment. By definition nanoparticles constitute a sub-fraction of what

is defined as ‘‘colloids’’ by the IUPAC. Since the definition of colloids and nanoparticles is based on a simple spatial dimension of an object, the variety of colloids and nanoparticles found in the environment is large, and the composition of environmental colloidal systems is complex and heterogeneous. A colloidal system is in general a two-phase system made up from a dispersing medium and a dispersed medium, and both may be gas, liquid or solid. Widely known are dispersions (solid in liquid), emulsions (liquid in liquid) and aerosols (solid in gas). In nature the dispersing medium is mainly water and air, while the dispersed media are mainly solids of inorganic, organic or biological origin or mixtures of. Aqueous dispersions and aerosols are hence the dominating colloidal systems in the environment. This, however, neglects the huge pool of colloidal particles that are bound in soils and sediments as aggregated structures and from where aggregates and single colloids can be released. Colloids in the environment can be of natural origin, formed by processes taking place for millions of years, or of anthropogenic . Atmospheric colloids may be produced by combustion processes, emitted as by-products in technological processes, by accidental and intended release, but will once settle and become a part of the terrestrial and aquatic environment. Nevertheless, colloids may be transported over large distances in the atmosphere and even naturally produced structures similar to carbon nanotubes have been found in thousands of years old samples from ice-cores of the arctic. Depending on their origin environmental aquatic colloids can be divided into four groups. Additionally, to the categorization developed by others. we distinguish anthropogenic from engineered nanoparticles according to their nature as an unintended by-product from technological processes and on the other side resulting from target-oriented manufacture. Subgroups are examples of environmentally relevant types: inorganic nanoparticles and organic nanoparticles. There has

therefore been a recent drive to define more closely nanoparticles, especially engineered nanoparticles (ENPs). There have been several reports on nanoparticles and nanotechnology. It is generally accepted that whilst the definition of other small particles often uses a simple scale to define size, in the case of nanoparticles, such a simplistic definition overlooks their unusual and diverse properties. This has led in some cases to the use of the properties of the materials as a key defining factor regarding the material, which is now being suggested [1].

1.2 The problem

There usage a little Known of the properties and behavior of non-particle in the environment and education. So it was very important to predict their find fate and behavior.

1.3 The aim

To study the optical properties for Nano- sized silicon dioxide.

1.4 Methodology

Preparing the sample of Nano- sized silicon dioxide and using X R Diffraction to study the optical behavior.

1.5 Literature Review

❖ Raman spectral study of silicon nanowires by Bibo Li, Dapeng Yu, and Shu-Lin Zhang Raman[2] .

spectra of silicon nanowires (Si NW's) have been analyzed, and the observed Raman peaks were assigned. The typical features of the first-order Raman peaks of the optical phonons were found matching those predicted by the quantum confinement effect. However, the sizes of Si NW's, derived from the microcrystal model (MCM) of Raman spectra do not fit the usual confined size, the diameter, of the nanowires from transmission electron microscope images. Abundant structure

defects can be observed in Si NW's so that the Si NW's actually consist of many smaller Si grains. The size of such Si grains was found to give a better agreement with the size derived from the Raman spectra. This indicates that MCM can be used to interpret the Raman spectrum of Si NW's as long as one takes into account the influence of defect on the confined size.

❖ Metal oxide nano-crystals for gas sensing by Elisabetta Comini [3].

Their use as gas-sensing materials should reduce instabilities, suffered from their polycrystalline counterpart, associated with grain coalescence and drift in electrical properties. High degree of crystallinity and atomic sharp terminations make them very promising for better understanding of sensing principles and for development of a new generation of gas sensors. These sensing nano-crystals can be used as resistors, in FET based or optical based gas sensors. The gas experiments presented confirm good sensing properties, the possibility to use dopants and catalyzer such in thin film gas sensors and the real integration in low power consumption transducers of single crystalline Nano belts prove the feasibility of large scale manufacturing of well-organized sensor arrays based on different nanostructures. Nevertheless, a greater control in the growth is required for an application in commercial systems, together with a thorough understanding of the growth mechanism that can lead to a control in Nano-wires size and size distributions, shape, crystal structure and atomic termination.

❖ Optical studies of the structure of porous silicon films formed in p-type degenerate and non-degenerate silicon by C Pickering, M I J Beale, D J Robbins, P J Pearson and R Greef [13].

The detailed structure of porous Si (PS) layers formed in p-type wafers with resistivities 0.01-25 Omega cm has been investigated using reflectance, transmission, ellipsometry and photoluminescence techniques. Marked differences

were observed in the optical properties of PS formed in degenerate or non-degenerate Si and these results are correlated with the results of other techniques. The optical techniques together with effective medium modelling have been shown to be useful non-destructive methods for either assessment of PS density or detection of unsuspected phases. The degenerate PS layers consistently showed good retention of the single-crystal characteristics of the starting wafer, only c-Si and voids being detected. For these samples, good agreement was obtained between optical and gravimetric densities. However, the non-degenerate PS had much greater variability, with greater loss of crystallinity and significant incorporation of oxygen, due to partial oxidation having occurred on or immediately after anodisation. Oxide fractions have been determined both optically and gravimetrically, with up to 50% oxide being detected in some samples. Non-degenerate PS samples with high oxygen concentrations appeared to be in the form of a chemical mixture, SiO_x, from interpretation of the optical constants. Photoluminescence measurements together with the other techniques indicated a complex mixture of phases in the latter samples-voids, alpha -Si:O (And/or alpha -Si:H), an unknown amorphous phase and silicon oxide. This complex structure probably contributes to the observed instability of thick non-degenerate PS layers when heated in UHV as part of the cleaning procedure prior to epitaxial growth, all degenerate samples being able to withstand heat treatment.

1.6 Thesis layout

Chapter one introduction

Chapter two silicon dioxide

Chapter three Nano particles

Chapter four Materials and Method

Chapter two

Silicon dioxide

2.1 Introduction

Sand (silica) – one of the most common minerals in the earth.

Main component in common glass:

•mixed with sodium carbonate and calcium oxide (lime) to make soda-lime glass for window panes, bottles, drinking glasses, etc.

Main component in optical fibers:

Crystalline SiO_2 is quartz

•fancy drink ware and artwork

•crystal oscillators using the piezoelectricity)

•Laboratory equipment [4].

2.2 The structure of the Silicon Dioxide

Tetrahedral arrangement with one silicon bonded to four oxygen atoms. Most oxygen atoms will be bonded to two silicon atoms, so that two tetrahedral are joined at a corner. (Bridging atoms) The orientation can be random, leading to an amorphous structure. Some oxygen atoms will be bonded to only one silicon atom (non-bridging atoms). The relative amounts of bridging to non-bridging determine the "quality" of the oxide. If all oxygen atoms are bridging, then a regular crystal structure results –quartz [5].

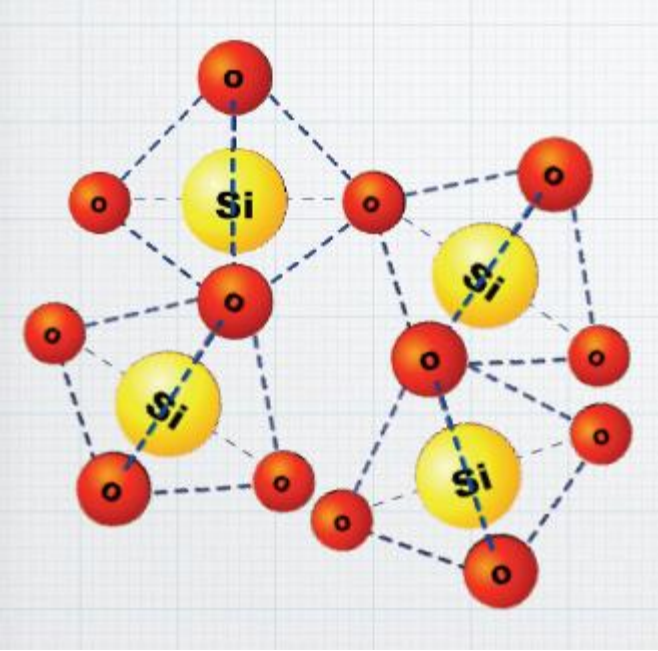

Figure 2.1 structure of SiO_2

2.3 The properties of the Silicon Dioxide

• In microelectronics, we use thin layers of pure SiO2. The layers are amorphous (fused silica)

• Density: (2.0 - 2.3) gm/cm^3

• Dielectric constant at low frequencies: εr = 3.9 (remember this!) refractive index at optical wavelengths: n ≈ 1.5

• Breakdown field: > 107 V/cm (1 V across 1 nm)

• The interface with silicon always results in electronic trap levels and some negative interface charge. Typical interface defect density ≈ 1011 cm^{-2}. This is not a high density of defects at an interface. It can be made even lower by annealing in hydrogen [5].

The combination of the relatively good electrical properties of silicon, the excellent insulating properties of SiO_2, and the low-defect interface between them is the key ingredient of modern integrated circuit electronics [11].

2.4 The Oxidation of silicon

There are several ways to form a layer of SiO_2 on the surface of silicon.

The two pre-dominate methods are:

• Thermal oxidation of silicon - react silicon from the wafer with oxygen to create oxide.

• Deposition of a thin film by chemical vapor deposition [5].

Thermal oxidation is a simple process - introduce an oxidizing atmosphere to the surface of the silicon with sufficient temperature to make the oxidation rate practical. There are two commonly used variants:

Pure oxygen: $Si + O_2 \Rightarrow SiO_2$ (dry oxidation)

Water vapor: $Si + 2H_2O \Rightarrow SiO_2 + 2H_2$ (wet oxidation)

Typical oxide thicknesses range from a few nanometers to about 1micron [6].

2.5 The Consumption of the silicon substrate

• In the reaction forming SiO_2, silicon atoms at the surface of the wafer must be converted to make the oxide. For a given volume of SiO_2 that is formed, a corresponding volume of the silicon substrate is lost.

• In crystalline silicon, each silicon atom corresponds to a volume of $2x10^{-23}cm^3$ (= 0.02 nm^3). In SiO_2, each silicon atom corresponds to a volume of about $4.4x10^{-23}cm^3$, depending on the density of the oxide,

or about 2.2 times more than the volume in the silicon.

• However, as the SiO_2 is forming, it cannot expand in all directions equally – it is constrained in the plane of the wafer. So all of the volume difference is taken up by expansion in the vertical direction [6].

Thinking about this in reverse, for a given thickness of oxide, *tox*, the fraction of the thickness that corresponds to consume silicon is 1/2.2 or 0.455. So, growing the oxide, we convert 0.455*tox* of the silicon thickness to oxide, and the grown oxide extends 0.545*tox* above the original surface of the silicon.

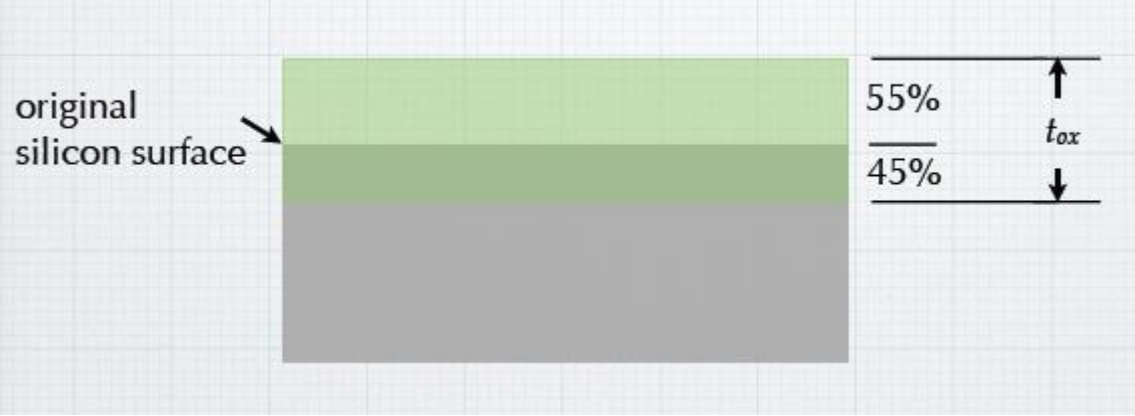

Figure 2.2 original silicon surface

2.6 Steps at the surfaces and interfaces

Grow an oxide layer. Then pattern and etch away the exposed region.

Figure 2.3 Grow an oxide layer.

Then grow a second oxide layer. The oxide in the exposed region grows faster than in the other area [6].

Figure 2.4 Grow a second oxide layer.

Steps are created at both the oxide surface and the Si/SiO_2 interface.

2.7 The Properties

2.7.1 Optical performance

Due to the low PL quantum yield (QY) of amorphous Si NPs, which is less than 2%, most researches focused 088102-6 Chin. Phys. B Vol. 23, No. 8 (2014) 088102 on the size-dependent and efficient PL of Si Nano crystals, the special optical properties, including bright emission, photo-stability, size-dependent and wavelength-tunable luminescence, and long fluorescence lifetime make them suitable for many applications. Although so far, the origin of PL is controversial and this question has no satisfactory answer, there is a consensus that the PL is generally determined by two aspects: one is due to the quantum confinement effect which may be the consequence of size quantization of the Si nanoparticle skeleton structure, and the other is assigned to localized states surrounding the nanoparticles. In the quantum confinement region, the PL property is closely dependent on dot size which is more important than surface chemistry in predicting the electronic properties of surface-passivized nanostructures, even with a 0.1nm change, which may lead to apparent differences in emission band energy. The PL peak will be red-shifted with size, increasing up to a size point larger than the

critical size point. Ledoux et al. explained the relationship between optical peak energy and particle size based on the quantum-confinement model using a linear combination of atomic orbitals (LCAO) (Fig. 2.5(a)), which has a recombination energy of the electron–hole pair (Eg), has a blue-shift with respect to the band gap of bulk Si (E_0 = 1.17 eV) and obeys an inverse power law with an exponent of 1.39 for the diameter (d) measured in nanometers (solid line in Fig. 2.5(a)) [6].

$$\mathrm{Eg(eV)(d)} = \mathrm{E0(eV)} + \frac{3.73}{d(nm)^{1.39}} \qquad (2.1)$$

Most part of the experimental data are in good accordance with the theoretical ones except some distinctions between data and theoretical results at both ends. For small particles, the deviation is attributed to the finite size distribution and the existence of an oxide-related surface state within the band gap of the Si Nano-crystals. Meanwhile, size dispersion is also a crucial factor, owing to the fact that when the size distribution becomes wider, the PL intensity will turn lower. Meier et al. systematically explored the influence of size distribution on optical emission performance. By using the equation [6].

$$I(\hbar\omega) = \int_0^\infty f_{osc}(\tilde{d}) \frac{d_n(\tilde{d}, d_0, \sigma)}{d\tilde{d}} I_{NP}(\hbar\omega, E_{g,\Delta E}(\tilde{d}) d\tilde{d} \qquad (2.2)$$

where s is the geometric mean deviation of Si NPs, f the oscillator strength, ¯hw the photon energy, D_n the spectral width of a single NP at room temperature, which acts as an in homogeneously broadened emitter, and I_{np} the PL intensity for a single particle, Meier et al. computed the PL emission of a NP ensemble with an average particle diameter d_0, and

they found that the model calculation fitted well with experimental data. So based on this, they kept the particle size d at a constant value and found the influences of

DE and son PL performance, which are shown by Fig.2.5(b)): the PL spectral shape is very sensitive to the particle dispersion s, even only a difference of 0.05 may lead to a significant change in

PL performance, that is, for small NPs, size distribution is an indispensable factor in deciding the PL.

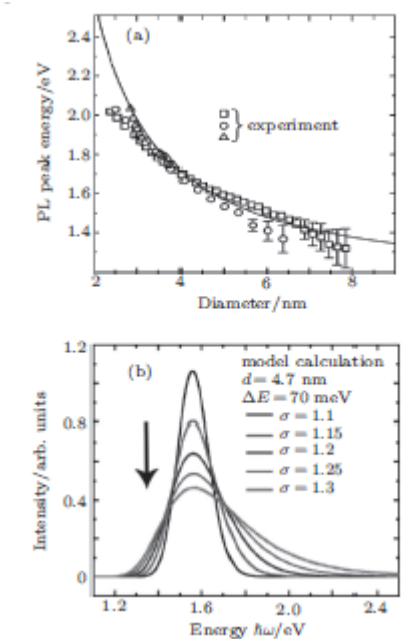

Figure 2.5 (a) Correlation between average diameter and PL peak energy.

(b) Correlation between the geometrical standard deviation on the ensemble PL spectral [6].

It has been widely known that the presence of oxygen or some other elements such as nitrogen can induce dramatic changes of PL properties. Recently, by capping $(E_tOH)/H_2O_2$ solution, Kang et al. were able to synthesize the Si cores in different sizes with a SiO_xH_y shell and showed a marked blue shift of emission wavelength from salmon pink to blue (Figs. 2.6(a) and 2.6(b)). Oxidizing the hydrogen-passivized surface of Si QDs in different times ranging from 0.5 h to 24 h led to diameter divergence from 3.0 nm to 1.2 nm (Fig. 2.6(c)), Kang et al. concluded that with increasing oxidation time, the Si core size significantly decreased which

was responsible for the finely wavelength-tunable emission photoluminescence. After the oxidation treatment, the PL QYs increase since the nonradioactive surface states are removed by the native oxide and simultaneously the emission energy shifts toward a higher band, accompanied by the shrinkage of the silicon crystalline core as a result of the surface oxidation. Through slowly heating or photo initiating, a SiO2 layer formed which was responsible for the conversion of emission colors. By post-treatment of high pressure water vapor annealing after oxidation passivation, the intensity of blue emission can be efficiently enhanced due to the inducement of the high quality of the Si–O–Si bridge or Si/SiO_x interfaces. Besides, trace nitrogen may also contribute to blue emission. Dasog et al. found two situations in which no blue PL was observed from the presented Si NPs synthesized by hydrofluoric acid etching of Si/SiO2 and they attributed this phenomenon to a charge-transfer-based mechanism raised by Nekrashevich and Gritsenko who explored the electronic structure of silicon oxynitride. In view of their various fabrication methods, Si Nano crystals can lead to different origins of blue PL. Yang et al demonstrated that Si NPs prepared by laser ablation in a liquid could emit blue light and featured aging-enhancement. They included a set of processes to explain the mechanism of blue light emission instead of a mere quantum confinement effect, that is, excitons were first formed through direct transitions at the G or X point by the absorption at 365 nm or 270 nm, and then partly trapped in nonradiative Pb centers, the others migrated to the near-interface traps at the interface between Si and SiOx ($0 < x < 2$). Besides the effect of particle size, size distribution, and an added element such as oxygen and nitrogen, surface characteristics can also lead to distinct changes of the optical properties of Si NPs. By capping the surface with various functional groups, compared with organic fluorophores and polysilanes, Si NPs maintain stable PL for a longer lifetime

which means it can effectively resist against photo bleaching. By comparing hexyl, octyl, dodecyl and octadecyl capped Si NPs; researchers found out that there was no obvious difference in optical properties among them when using different length chains. Moreover, there were also some cases concerning PL enhancement through surface modification. Through surface derivation of diphenylamine and carbozale separately, Li et al. produced ultra-bright Si QDs with the stable QYs up to 50% and 75%, respectively, due to a single highly emissive recombination channel across the entire NP ensemble induced by the modification. Meanwhile, the emission peak was red-shifted from 405 nm to 500 nm. In contrast, (3-aminopropyl) triethoxysilane (APTES) derived hydroxyl-terminated Si NPs presented a distinctively attenuating PL intensity and a blueshift due to the polarity characteristic of amino group. The QYs of Si NPs conjugated with different functional groups are summarized in Table 1[7].

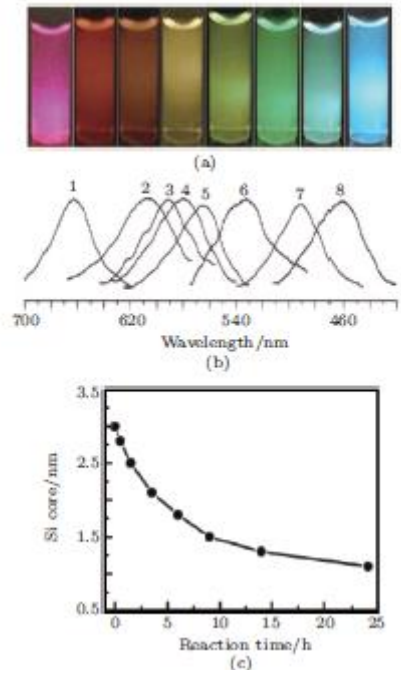

Figure 2.6 (a) Photograph (under UV light) of H–Si QDs (left, red emission)

and seven water soluble Si QDs (yielding seven distinct emission colors)

(b) PL spectra of H–Si QDs (curve 1) and Si QDs of 0.5, 1.5, 3.5, 6, 9, 14, and 24 h oxidization (curves 2–8), respectively (excitation wavelength: 360 nm).

(c) Plot of the oxidation time versus Si core size.

Functional group	Synthesis route	PL QY/%	Size distribution/nm	Medium solution
Octasiloxane[10]	reduction of $SiCl_4$	12	3.28±0.86	hexane or chloroform
Allylamine[41]	reduction of $SiCl_4$	10	1.5±0.5	water
Octylamin[48]	reduction of zintl salt	18	3.9±1.3	water
3-aminopropenyl[30]	microwave-assisted reaction in liquid	15	3.4±0.7	water
Immunoglobulin G (a protein)[73]	microwave-assisted reaction in liquid	18	3.17±0.53	water
Dodecyl[87]	reduction of micelle	14	6.05±1.94	hexane
Aminoalkyl[51]	microwave-assisted reaction in liquid	20–25	2.2±0.7	water
Octanethiol[24]	degradation of organosilane	5.5	4.64±1.36	water

Table 2.1 QYs of Si NPs conjugated with different functional groups.

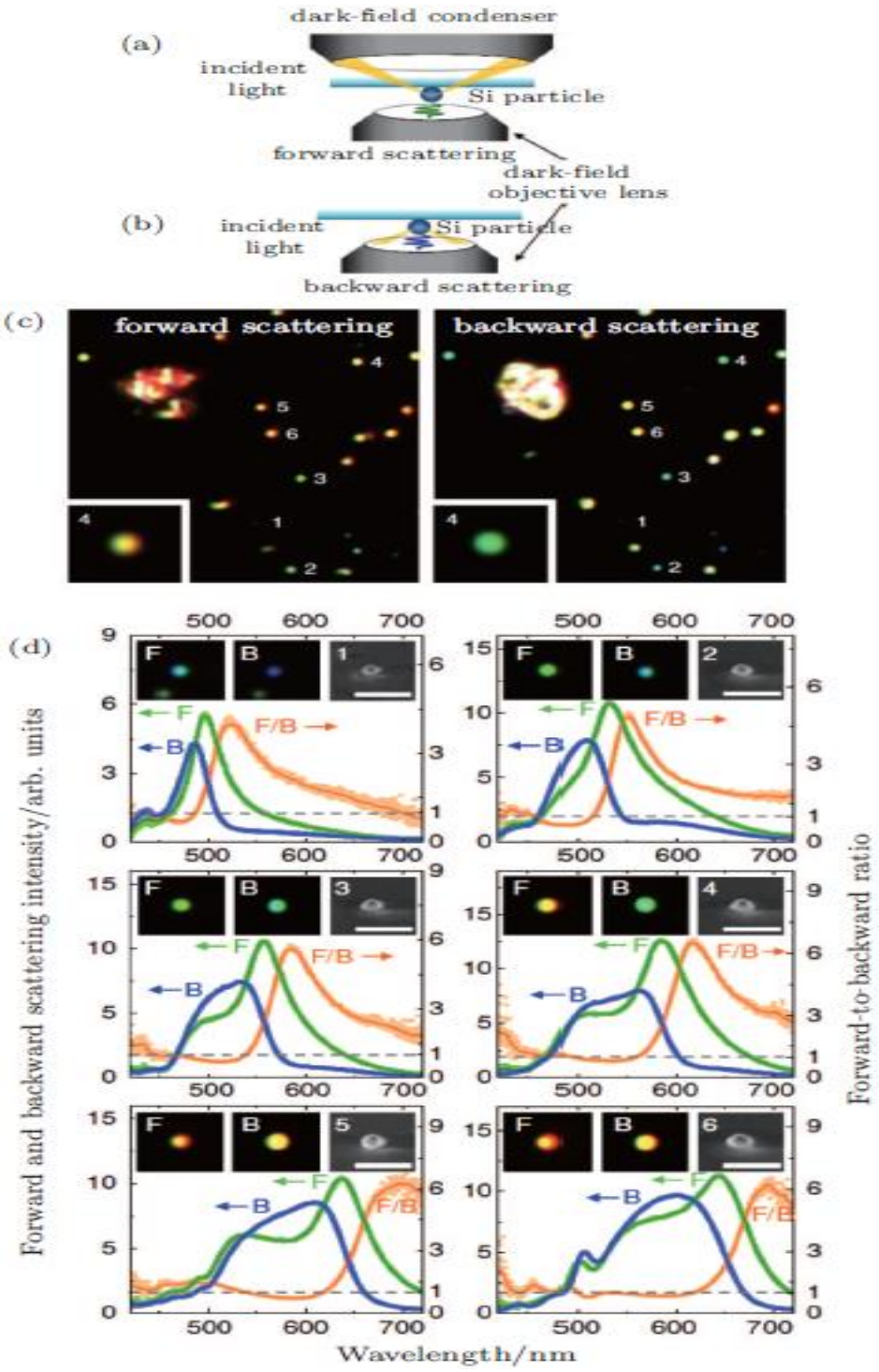

Figure 2.7 (a) and (b) Schemes of forward and backward measurements.

(c) magnified dark-field microscope image of nanoparticle

(d) Left axes show forward (green) and backward (blue) scattering intensities,

Nowadays, Nano composites (e.g. Si NPs/magnetite, Si NPs/silver) have attracted considerable attention, for their multi-functionality is superior to either component. Martens et al. have synthesized Si NPs coupled with silver rods, and the nanostructure can extremely enhance the PL intensity which is attributed to the electromagnetic coupling of the Si QD emission dipoles with dipolar plasma modes in the silver rod. Iron-doped porpylamine-terminated Si nanoparticles have been fabricated for both photoluminescence and magnetic resonance imaging (MRI) detection. In this study, a sample containing the least quantity of iron (Si1Fe) exhibited the highest QYs (15%); a higher concentration of iron dopant (Si5Fe) caused fluorescence attenuation (10%), whereas MRI T2 contrast increased. Besides the influence of iron content, it has been found that the size of the hybrid is another significant factor influencing the intensity of PL. Besides the controllable PL, recently, directional anisotropic scattering in the visible spectral range of Si NPs has been explored in depth, in order to apply Si NPs to some emerging Nano-scaled applications. Based on the theoretical modeling by using Mie theory, Fu et al. synthesized approximately spherical Si NPs solidified on glass substrates with thickness values ranging from 100–200 nm and systematically analyzed the scattering performances in the forward and backward directions (Figs. 2.7(a) and 2.7(b)). As shown in Fig. 2.7(c), labeled samples manifest various scattered colors in two directions due to simultaneously excited electric and magnetic dipoles. By comparison with the measured spectral behavior of the six Si NPs (Fig. 2.7(d)), Fu et al. also confirmed that the quasi-spherical Si Nano crystals could act as ‘Huygens’ sources and the spectral region was tunable since the scattering resonances was merely linearly dependent on the particle size and wavelength of the illumination light [7].

2.7.2 Electronic properties

Generally, special PL properties of Si NPs are primarily due to the quantum confinement effect caused by the restricted size at the nanoscale. The existing quantum confinement model is closely related to the size-dependent band gap which is also one of the major characteristics of electronic nature. According to the research results presented by Van Buuren et al. after synthesizing Si NPs with a fair size range from 1–5 nm, they found that the valence band (VB) edges of the Si Nano crystals shifted down by 0.5 eV with respect to vacuum level, owing to electronic structure changes caused by quantum confinement. Moreover, the conduction band (CB) shift was measured as a function of the VB band shift which is quantitatively equal to twice the former. They confirmed the inverse relation between particle size instead of geometric shape and the size of the band shift. However, the calculated band gap did not perfectly match the measured one due to the partially oxidized surface and substrate–cluster interaction. In addition to the marked effect of particle dimension on electric performance, the type of dopant (phosphorus or boron), composition material, surface functionalization and post treatment similarly manifest noticeable effects. For example, by comparing the electronic transport of Si NCs networks using films composed of P-doped Si–NCs with those using films consisting of Si NPs without doping elements, Stegner et al. found that the dopant can strongly influence the electronic transport properties of the films. For the undoped film, thermal activation energy (Ea) was about 0.5 eV and the increased dopant concentration led to the relationship that conductivity increases and conductivity decreases as temperature rises. Apart from these, Kim et al. adopted plasma-enhanced chemical vapor deposition (PECVD) followed by annealing to insert Si NCs into amorphous silicon nitride to prepare silicon-based solar cells. However, the large spacing between Si NCs in silicon nitride film

brought about lower light absorption-induced photocurrent than the theoretical value, from which one can conclude that the spacing relationship between Si Nano crystals was also a remarkable factor influencing the electric properties [7].

2.8 Applications

2.8.1 Light-emitting applications

For light-emitting applications using Si NPs, most of them rely on their robust electroluminescence (EL) potential. The realization of this application demonstrated that through optimizing the confinement of holes and electrons of the Nano crystal layer, the semiconductor material can also be used in this field. Work by Maier-Flaig et showed that through using monodispersed size-separated silicon nanoparticles, multicolor silicon-based light-emission diodes (Si LEDs), featuring long-term stable EL as well as widely tunable colors ranging from deep red to orange–yellow, can be achieved. The Si NPs proved to play a pivotal role since the emission characteristic substantially originates from it through the comparison between EL and PL spectra. Moreover, the increasing external quantum efficiency (EQE) is partially determined by the reduced thickness of the Si NP layer and the high wavelength emission of Si Nano crystals. Meanwhile, comparative trials have been carried out between samples with and without size selection. The results showed that a longer operation time of the device results in superior particles as indicated by the comparison between 40-h and 15-h operations. Simultaneously, the products with selected Si NPs could realize small voltage-dependent wavelength shifts of the order of 15 nm when the applied voltage was increased from 3.5 V to 10 V, which is attributed to the residual size distribution. In addition, the device also displayed some particular merits, e.g. extreme brightness with the QYs up to 43%, low turn-on voltage of approximately

2 V for red-emitters, and thus paved a perfect way to new silicon-based optoelectronic applications [8].

2.8.2 Applications in the energy and electronic fields

Si NPs exhibit fascinating electronic and optical properties compared with bulk silicon and have been investigated in depth for photovoltaic applications. For lithium ion battery applications, silicon formulations such as silicon Nanowires, silicon nanotubes and micro porous silicon nanoparticles have been widely investigated to overcome the disappointing shortcomings of previous silicon anodes. Despite the change in nanostructure, researchers have Ceaselessly been searching for novel candidate anode materials featuring higher Li-ion storage and stronger rechargeable capability to serve as substitutes for low charge-stored carbon-based anodes. Recently, Guo et al. focused on synthesizing a Si/C Nano composite by infiltrating the Si NPs uniformly into the carbon matrix in order to excite its potential as anode material. To prove the superiority of this micron-sized mesoporous Si–C Nano hybrid, delithiation capacity, columbic efficiency (CE) and a charge/discharge process were systematically discussed. The resulting curves show that, except for the depressing irreversible capacity for the initiate cycles with a CE of only 22.3%, with the increase of cycle number the delithiation capacity shows a desirable increasing tendency until the 70th cycle, after which it maintains a high level constantly. Researchers attributed this phenomenon to the partial existence of a SiOx layer, through which the Si NPs can disperse in the carbon precursor homogeneously[8].

Despite the manifestation of deformity in the first cycle, this lithium battery anode in which Si NPs plays a vital role is a significant leap in this field for its prominent cycling stability and high reversible capacity. Ge et al. synthesized a novel

grapheme oxide-wrapped carbon coated porous silicon nanoparticle anode featuring better cycle-ability and less capacity degradation, for it could operate at much higher current rates of 1/4 C and 1/2 C and deliver extremely stable capacities of 1400 mA.h/g and 1000 mA_h/g after 200 cycles, respectively fig 2.8.

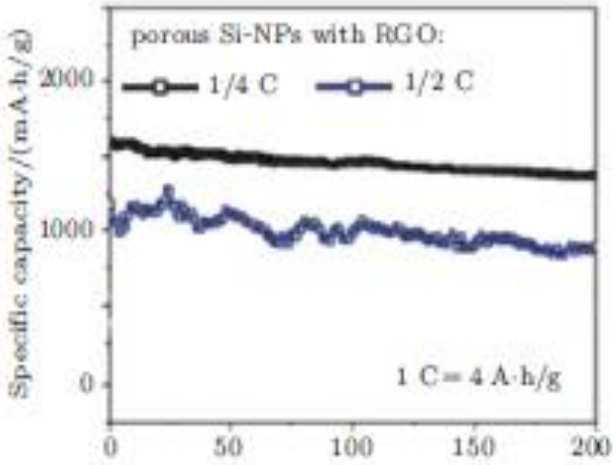

Figure 2.8 (color online) Cycling performances at current rates of 0.25 C and 0.5 C

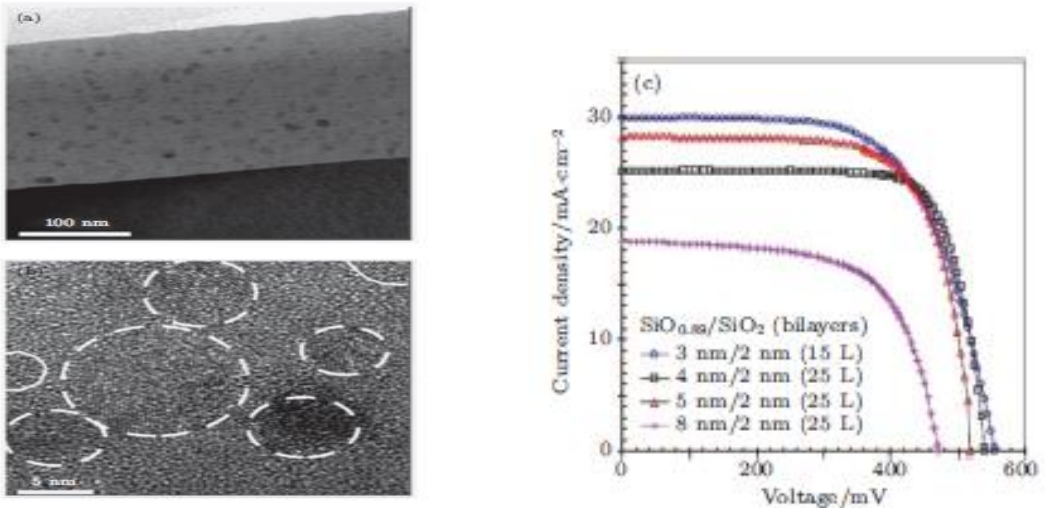

Figure 2.9 (color online) TEM images of Si QDs in an SiO_2 matrix,

(a) low-magnification image and

(b) high-resolution image.

(c) One-sun illuminated I–V curves of four different (n-type)

Si QD/ (p-type) c-Sisolar cells measured at 298 k

For solar cell battery applications, there are several nanostructured cell protocols to achieve higher conversion efficiency than those protocols based on a single p–n junction such as silicon-based tandem cells, hot carrier cells and up- and down conversion. Recently, Cho et al. reported that they have successfully fabricated a phosphorus-doped Si QD super lattice as an active layer on a crystalline silicon oxide substrate as a heteroface solar cell. For its high solid solubility in silicon under high annealing temperature (1100 C), phosphorus was chosen to be the alloying element to form P-doped Si QDs by magnetron sputtering of Si, SiO_2 and P_2O_5 targets. The structures are shown in Figs 2.9(a) and 2.9(b). Through comparing heteroface diodes with different Si NPs diameters, the cell with 3-nm

QDs capped with a 2- nm SiO_2 layer was described as being superior for its higher open-circuit voltage (Voc), short-circuit current (Jsc) and conversion efficiency under solar illumination over other counterparts (Fig. 2.9(c)). For electronic devices, since 1999 when Ridley et al. reported the first nanocrystal field-effect transistor (FET) prepared by using sintered CdSe NCs, FET containing Si NPs have attracted great attention. Recently, there was a report concerning Si NPs thin-film field-effect transistors prepared from solution. In this article, Si NCs were synthesized in a nonthermal plasma via the dissociation of hydrogen and SiH_4; the resulting powder was dissolved in 1, 2-dichlorobenzene (DCB) followed by sonication, thus forming a stable suspension, though it was not optically transparent. To have a comprehensively understanding, germanium NP-based FET was also studied. The two kinds of bottom-gate FETs were fabricated by spinning them onto $Au/Si_2+/SiO_2$ substrates, the structure is shown in Fig. 2.10(a). Unlike the Ge-based apparatus, films of Si NCs of either 4 nm or 7 nm in diameter exhibit n-type behaviors (Figs. 2.10(c) and 2.10(d)), but have a nonuniform, discontinuous and visible rough surface (Fig.2. 10(b)), though it manifested poor performance, for the on-to-off ratio is approximately two orders of magnitude and the transfer curve shows significant hysteresis. It was the first time to realize deposition of Si NC thin films from solution which showed gating without any post deposition treatment [8].

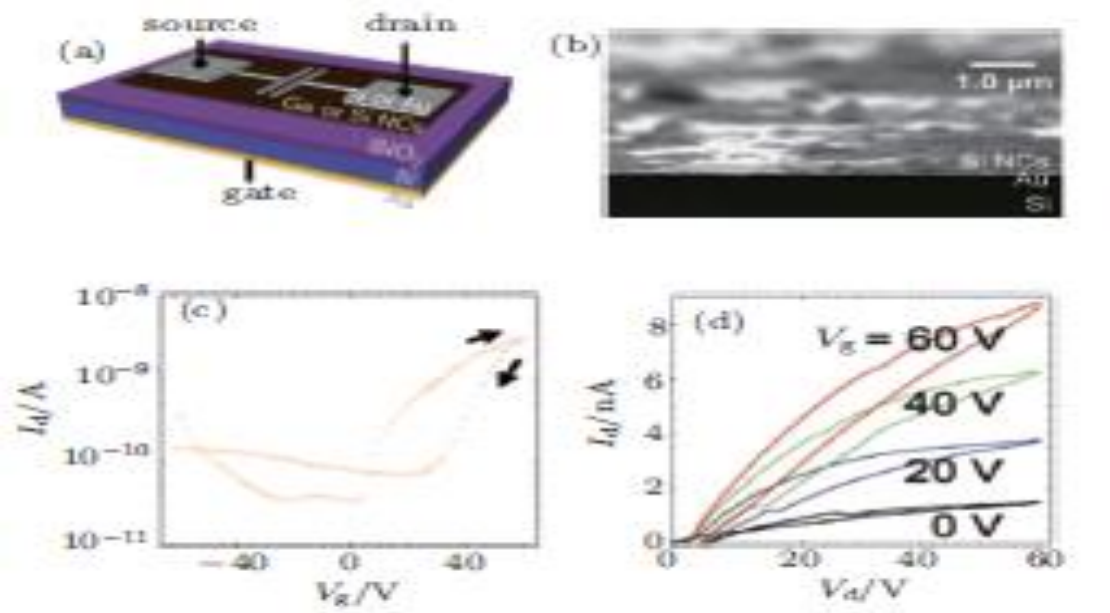

Figure 2.10 (a) Schematic plot of FET device. The channel dimensions are 200 _m_2000 _m and the source is grounded during (b) A 7-nm-thick Si NC film on an Au-coated Si wafer. (c) Drain current (Id)–gate voltage (Vg) for two different (10–20) nm asdeposited Si NC FETs. (d) Drain current (Id)–drain voltage (Vd) characteristics for two different (10–20) nm as-deposited Si NC FETs

2.8.3 Photo catalysts

Heterogeneous Nano catalysis is a fascinating field in nanotechnology. Although numerous kinds of metal oxide and sulfides have been investigated and improved by changing the chemical composition, surface fabrication and energy gap, silicon nanostructures, such as H-terminated nanowires, porous silicon nanowires and silicon nanoparticles also win a space in this domain for themselves. In this respect, our group has already successfully prepared silicon QDs with dimensions of (1–4) nm by high energy ball milling (Fig. 2.10(a)) and concluded that the pure

Si NCs without any capping of molecules on their surfaces exhibit excellent rates for conversion of carbon dioxide into aldehyde. By quantifying the concentration of the resulting formaldehyde by adding Nash reagent to samples and monitoring its maximum absorbance at 412 nm under three contrast tests (Fig. 2.10(b)), we found that the exposed Si QDs can serve as efficient photocatalysts for effective recombination between electrons/holes induced by photons and CO_2/H_2O, respectively[9].

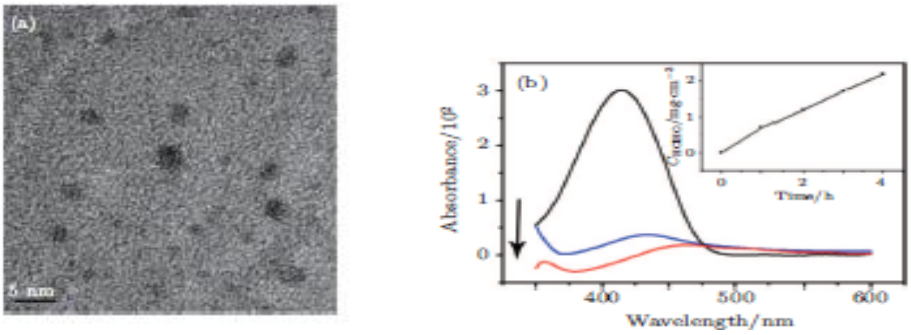

Figure 2.11 (color online) (a) TEM image of Si NCs produced by HEMB for 3-h illumination. (b) UV–visible spectra of the reaction solution (after 2-h illumination) treated with Nash reagent for the determination of formaldehyde. As the arrow indicates, from the top to bottom, the line represents obtained UV–visible data in the presence of unmodified Si NCs with illumination, in the absence of illumination and in the absence of unmodified Si NCs, respectively. Inset: the concentration of formaldehyde as a function of reaction time

By following an electrochemical etching recipe, (1–2) nm and (3–4) nm Si QDs were prepared respectively by Kang et al. Here, they demonstrated that CO_2 reduction and dye (methyl red) degradation can be effectively proceeded by utilizing (1–2) nm Si QDs serving as an excellent photo catalyst, whereas (3 – 4) nm QDs are for the selective oxidation of benzene instead of the reduction of CO_2/

H_2O or the degradation of methyl red (Fig. 2.12). The striking difference between them may be due to the larger electron/hole pair energy of (1– 2) nm Si QDs than that of (3 – 4) nm Si QDs which is responsible for its limited usage. Despite this, (3 – 4) nm Si QDs can potentially function as a photocatalyst for the hydroxylation of benzene by H_2O_2. In this process, the (Si–SiO_x) core–shell structure stemming from partially oxidized H-terminated Si QDs actually fulfilled its photocatalytic duty, on which H_2O_2 molecules were absorbed and decomposed into active oxygen species with oxene characteristics, which were electrophilic and prone to oxidize benzene rings into phenol and simultaneously the photoelectron reductive atmospheric protected it from further oxidizing which might lead to high selectivity of phenol formation.

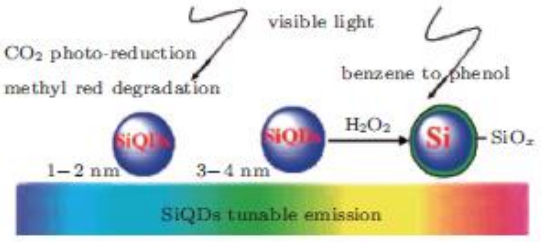

Figure 2.12 (color online) Schemetics for Si QDs of different diameters from different reactions [9].

2.9 Summary and prospects

The strategies to synthesize silicon nanoparticles, utilizing different apparatus and chemical compositions, have advanced significantly during the past 50 years. There are numerous synthesis routes for silicon Nano crystals featuring distinctive Characteristics. Physical processes generally produce limited yields of pure products but can get rid of contaminants originating from byproducts. While chemical routes tend to scale up the yields and complete further functionalization

synchronously, they are plagued by impure products. Efficient modification methods based on different exterior bonds such as Si–H, Si–Si, Si–C, Si–OH can significantly lead to a better understanding of its essential optical and electric properties. This article also discusses a range of applications which are rapidly developing and have extended to broad fields. Among these, we focus on exploring their potential in energy and biomedical applications, and as Nano catalysts—all show a promising future. Despite the fact that there are already myriad researches on Si QDs, the natures of certain properties are still unclear. So, more investigations are necessary to confirm whether there are any other theories except quantum confinement and oxide related defects, which can grasp the comprehensive principles to explain some amazing phenomena such as PL quenching when sensing some chemical molecules. Other potential avenues of research may include improvements in synthetic strategies to produce stable silicon colloids dispersed in a wide range of solvents instead of the given one, and to reliably fabricate controlled particles with an appropriate size and biochemical Functional groups for more extensive applications. There is no doubt that the attention paid to the field of Si NPs will increase—more creative research results are expected to be presented—and this material will have an immeasurable influence on the future society [9].

Chapter three

Nanoparticle

3.1 Introduction

Nanoparticles are particles between 1 and 100 nanometers (nm) in size with a surrounding interfacial layer. The interfacial layer is an integral part of Nano scale matter, fundamentally affecting all of its properties. The interfacial layer typically consists of ions, inorganic and organic molecules. Organic molecules coating inorganic nanoparticles are known as stabilizers, capping and surface ligands, or passivating agents. In nanotechnology, a particle is defined as a small object that behaves as a whole unit with respect to its transport and properties. Particles are further classified according to diameter [10].

3.2 Nanoparticle structure

Although it is often tempting to consider nanoparticles as simple molecules, they are in fact complex mixtures. Even in the simplest cases one must consider the interactions of at least two different aspects of the material. Whilst they may absorb light like a dye and appear to dissolve like any

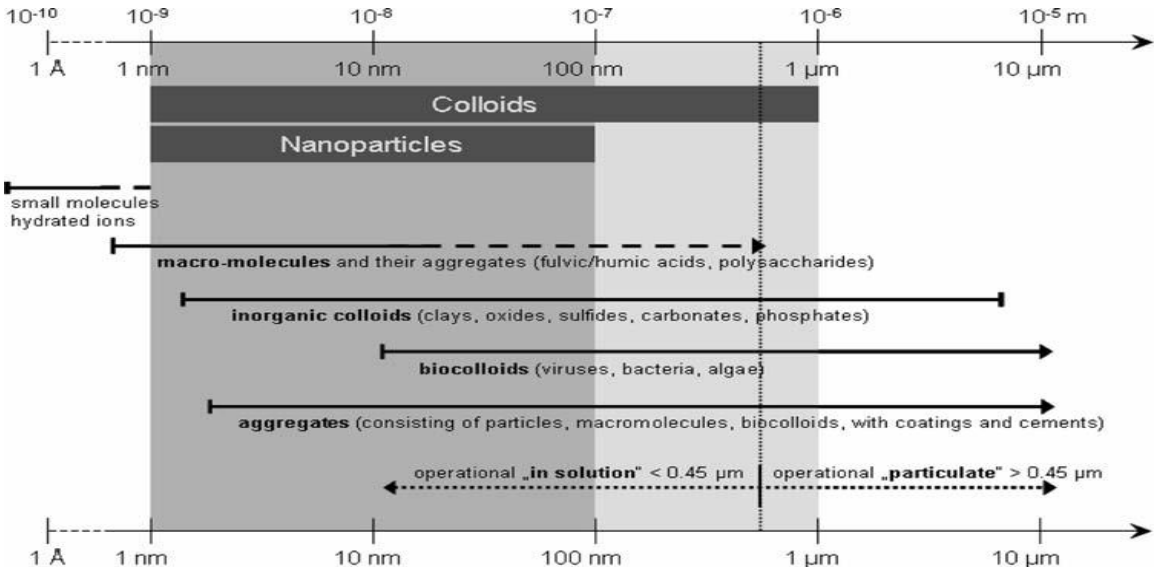

Figure 3.1 Size domains and typical representatives of natural colloids and nanoparticles. Operationally defined cut-off is given for filtration at 0.45 lm

environmental aquatic colloids				
natural colloids		anthropogenic colloids	engineered nanoparticles	origin
inorganic colloids - silicates (e.g. clays) smectites montmorillonite nontronite hectorite chlorites mica kaolinite - oxides / hydroxides Fe-oxohydroxides Mn-oxides - carbonates - phospates - metal sulfides - polym. silicic acid	organic colloids - macromolecules humic acids fulvic acids polysaccharides proteins peptides exo-polymers, EPS - bio-colloids bacteria viruses fungi - coal/soot/black carbon - cellular debris	wear & corrosion products - from tire & brakes - from catalysts (e.g. Pt, Pd) - metals (wear in bearings) - metal oxides (roof run-off) - additives to lubricants waste & combustion products - soot - "anthropogenic" humic acids from e.g. waste dumps - tar leachates in plumes - fly ash - fine dust (inorganic & organic)	standard industrial products - polymers - surfactants - dyes & pigments - metal oxides NP metals & metal oxides - metals (Au, Ag, Fe) - metal oxides (of Ti, Zn, Zr, Ce...) - metal tubes and wires carbon based - fullerenes - single & multi walled nanotubes hybride structures - quantum dots - functionalized materials - core-shell structures	composition

table 3.1 Categorization of environmental colloids according to origin and composition.

other small molecule, their actual behavior is often subtly different and is usually the result of the different components of the material. Any nanoparticle will have an exceptionally high surface area to volume ratio; this is one of the reasons for some of their unusual properties. However, this high surface area also means that the surface of any given nanoparticle is an important component of the material. So even the simplest nanoparticle will have a surface chemistry, which is distinctly different from that of the core material. In the case of silica, the material will have a core structure of SiO_2, but the surface would have a chemistry more comparable to a formula Si(O)(2-x) (OH)(2x). The result of this is that the outer layer of atoms in the particle has a different composition from the rest of the particles. One layer of atoms is approximately 0.4 nm thick; there is a significant number of atoms with a different chemistry from the rest of the atoms on the particle. This means that for a 6-nm silica nanoparticle, approximately 7% of the Si atoms will be on the surface, and therefore the surface chemistry of the particle will have a significant contribution. Furthermore, the surface of the nanoparticle will be the first aspect experienced either by the environment or by an organism. In many cases the exact composition of the surface of the nanoparticle is intimately related to their final application. For example, a nanoparticle designed to interact with biological systems will have suitable functional groups attached to its surface, such as short chain peptides. In fact, in many cases the surface functionalization is critical to producing nanoparticles that exhibit the correct properties. This is often due to the fact that many nanoparticles lose their unique properties once they have aggregated and precipitated from suspension. Great effort is therefore expended in preparing nanoparticles that suspend in the media of choice. This usually involves preparing nanoparticles that have some coating that facilitates dispersion of the particles. In some cases, these coatings are in the form of surfactants that form transient Van-

der-Walls interactions with the surface and exist in equilibrium with the free surfactant molecule. In other cases, a molecule or ion is bound to the surface of the particle so imparting stabilization of the particle suspension.

The modes of stabilization of colloids of this type will be discussed later.

A nanoparticle can therefore be split into two or three layers; a surface that may often be functionalized, a shell material that may be intentionally added and the core material. Often nanoparticles are only referred to by their core material because this is the part of the nanoparticle that results in key properties for most applications [10].

3.3 The surface

The surface of a nanoparticle may be functionalized with a range of metal ions, small molecules, surfactants or polymers. It is well known that the base catalyzed hydrolysis of tetraethyl orthosilicate results in particles of 10–350 nm that have a charged surface. This has been shown to be the result of deprotonating of the SiOH groups at the surface of the particle resulting in the formation of a SiO- M+ where M+ is a suitable monovalent cation such as sodium. Preparing a nanoparticle with a charged surface is aconvenient way to prepare nanoparticles that disperse in media. However, many materials do not have convenient surfaces for stabilization of localized charges. In many of these cases, it is common to use a small molecule that will bind to the surface of the particle by a covalent-like bond and also contain groups capable of carrying a charge. Citrate stabilized gold and silver sols come under this category. Similarly, thiopropanoic acid has also been used. Another method for preparing a stable dispersion of nanoparticles is to use a surfactant such as sodium dodecyl sulfate (SDS). In this case the nanoparticle forms in the core of a micelle with the hydrophobic interactions of the surfactant tail and the particle

surface drives the binding of the surfactant to the surface of the particle. It is important to remember these systems are different from those where a molecule is covalently bound to the surface of the nanoparticle in that the surfactant is in equilibrium with free surfactant molecules in the media. If the system is diluted, then this equilibrium will shift so that the concentration of the free surfactant is maintained at the critical micelle concentration. This equilibrium will shift as the expense of colloid stability and therefore excessive dilution will result in colloid instability and precipitation. A final type of surface-active molecule includes those based on nonfunctional long-chain molecules such as amines, phosphine's, carboxylates and thiols.

These molecules bind to specific sites on the surface of the nanoparticle and have long chains that extend into the dispersion medium, thereby imparting stability. Generally, these are applied to the surface of the particle during preparation and can be later modified. Often stability is limited to organic solvents although new materials based on polyethylene glycol (PEG) are now being prepared in our group. It is not unusual to prepare such materials for dispersion in hydrophobic solvents and then modify their surface with PEG in order to impart water dispensability [10].

3.4 The shell

This is a layer of chemically different material from the core material. In a sense the outer layer of any inorganic nanomaterial may be considered to be different from that of the core and therefore be considered to be a shell. However, the term shell is usually applied to a second layer that has a completely different structure from that of the core material as opposed to a serendipitous variation in chemistry due to being at the top layer of the particle. Some excellent examples of these

materials are the core/shell quantum dots, which contain a core of one material, such as cadmium selenide, and a shell of another, such as zinc sulfide. Other examples may be drawn from polymer nanoparticles such as polystyrene-polyanaline. Whilst these types of material may be prepared intentionally, it does not imply that they can also occur through other processes. For example, it is well known that iron nanoparticles rapidly form layers of iron oxide at their surface after preparation. These layers do not necessarily penetrate the whole particle, and therefore the nanoparticle itself may be a core shell structure as opposed to a pure iron nanoparticle. These materials are usually prepared intentionally and are unlikely to occur serendipitously [11].

3.5 The core

This is essentially the Centre of the nanoparticle and usually used to refer to the nanoparticle itself. This trend is common in the physical sciences where the particular properties of a nanoparticle under study are generally related to the composition of the core, or in some cases the core and shell. However, there are examples where it has been shown that the exact composition of the whole nanoparticle is implicit in accurately determining its overall properties. It should be noted however that in general the properties of interest to the physics and chemistry communities are generally dominated by the properties of the core. However, the same rules do not necessarily apply to ecotoxicology. It is highly likely that the core of the nanomaterial will play a key role in the nanoparticle toxicity; however, this does not mean that the fate and environmental behavior of a nanoparticle will be dominated by core composition.

A second important consideration when discussing the core of a nanoparticle is the immense variation that may be found there. This is particularly the case when considering inorganic nanoparticles. It is well known that most inorganic materials

may exist in more than one phase and that the phase of the material may have a dramatic effect on its physical properties. Whilst nanoparticle may be prepared in a pure single phase, it is sometimes the case that two phases are present. It is tempting to assume that the fate and behavior of the nanoparticle are independent of the phase; however, this is also unlikely to be the case. Furthermore, even careful descriptions of nanoparticle can lead to misleading assumptions. For example, consider a collection of particles where the core material is TiO_2 with particle diameters of 30 nm (±10 nm) comprising 75% anatase and 25% rutile. These data could be considered to give a full description of the material. However, there are many ways to understand this description: a mixture of rutile and anatase particles with the same size distribution, a mixture of small anatase particles and large rutile particles (or vice-versa), a mixture of nanoparticulate anatase contaminated with a small amount of bulk ([100 nm) rutile, a collection of nanoparticles, each of which have a mixed phase composition of 75% anatase and 25% rutile in each particle, etc. It is tempting to interpret these data to mean the first case, however, given the difference in the chemistries of rutile and anatase this is probably the lease likely scenario. It is well known that, in nanoparticles, many crystal defects and other twinning and packing phenomena may result in very complex core compositions. Whilst it is impractical to analyses all materials for ecotox testing to these levels, it is important that these possible variations are born in mind so that they can be considered if some unusual results become apparent at a later date [11].

A final and more general consideration regarding nanoparticles should be their morphology. Whilst many nanoparticles which are already generally used are nominally isotropic, there is much other morphology which can be attained. Perhaps the most common is a simple rod or wire, such as a carbon nanotube

(CNT). However, tetrapod, tear drop, dumbbell and dendrite structures have also been prepared for a range of materials. Often control of these shapes is related to the phase of the components of the system, but also may be related to changes in composition of the materials themselves. Whilst very few of these materials have yet to find commercial applications, there is the obvious possibility that one day they will, and therefore the exact morphology of the nanomaterial will also become a much more complex issue. Intrinsic properties of nanoparticles The fate, behavior and therefore the ecotoxicology of nanoparticles will be closely related to their intrinsic properties. There are several aspects to nanoparticles which can easily be dismissed in error due to their apparent ability to behave more like molecules than larger colloidal suspensions. We will discuss here a simple description of particles in suspension [11].

3.6 Surface energy and colloid stabilization

The small size of nanoparticles would imply from simplistic calculations that they should form stable dispersions because they are subject to Brownian motion to a significant degree. However, this would be neglecting the high surface energy of the nanoparticles. Any collision event between two particles will result in agglomeration and precipitation of the nanoparticles from solution. It is therefore necessary to stabilize the dispersion of the nanoparticles by providing a barrier to close approach of two particles. Typical barriers are either based on charge or steric stabilization of the colloid. In the first case a charged surface is present which has associated counter ions and some solvent molecules which are tightly bound to the surface of the particle; this is called the Stern layer. The associated charge at the surface causes repulsion of like charges according to coulombs law so providing a barrier to aggregation (Fig. 3.2(a). In steric stabilization a relatively

long molecule is tethered to the surface of the particle. The long chain of the molecule will have a high affinity for the Solvent. The barrier to aggregation is therefore related to the relative interactions of the polymer chain with itself and with the solvent. In order for the particles to aggregate solvent must be eliminated from between the two particles and from around the chains; this is energetically unfavorable and therefore presents a barrier to aggregation (Fig. 3.2(b). These two types of stabilization may act very differently. For example, changes in ionic concentration have a dramatic effect on the stability of charge stabilized Colloids at much lower concentrations than sterically stabilized colloids. This is because the increase in ionic strength shields the charge of two approaching particles and reduces the effectiveness of the Coulomb repulsion. Furthermore, polyvalent ions may exchange for the

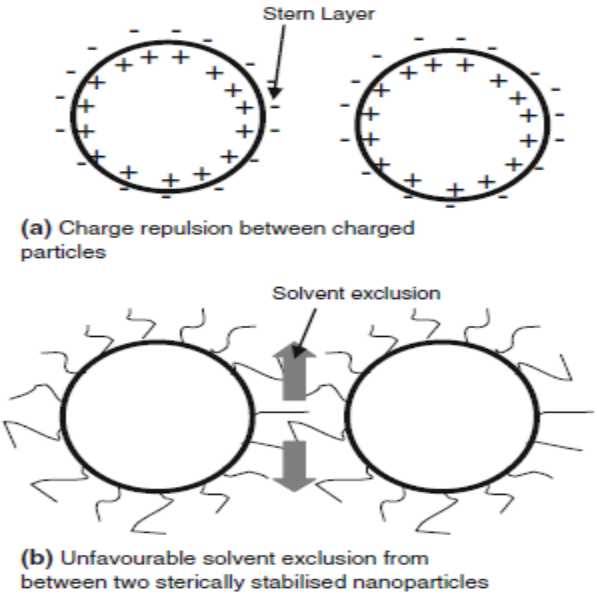

Figure 3.2 A diagrammatic representation of (a) a charged stabilized nanoparticle and (b) a sterically stabilized nanoparticle [11]

monovalent ions on the surface of charge stabilized colloids. This often results in rapid precipitation and aggregation of particles, whereas sterically stabilized systems are much less susceptible.

3.7 Optical properties of nanoparticles

One particular subset of nanoparticles is the quantum dot. These are generally particles with diameters of less than 10 nm, although in some cases the particle size may be as large as 50 nm. They have perhaps the most distinctive size-related properties of all nanoparticles. Quantum dots are semiconducting nanoparticles where their dimensions are so small the size of the particle affects the intrinsic band gap of the semiconductor. A simple way to understand this is to consider a semiconductor as consisting of a valence and conduction band which are the result of the bonding and antibonding configuration of the crystal lattice. A simple diatomic system will have a single bonding and a single antibonding orbital. As more atoms are added to the lattice the new bonds will have slightly different bonding and antibonding energies. For a large lattice these orbitals will begin to form a continuum which is considered as the band in the final bulk material. It is therefore clear that at some point the number of bonds in the semiconductor particle will not be a good approximation to an infinite lattice and the band structure will begin to change. This results in a widening of the bandgap of the semiconductor. Most quantum dots exhibit photoluminescent properties. A photon of incident light can excite an electron from the valence band of the semiconductor to the conduction band leaving a hole in the valence band. This photon then has various possible fates: recombination of the electron and hole with the emission of light, trapping of the electron/hole in a defect in the crystal, reaction with the capping agent resulting in the formation of a radical, reaction with the solvent to

form a radical. Many of these processes will also occur in particles which do not exhibit quantum confinement; however, the minimum energy required to form the excited state will increase as the particle size decreases in a quantum-confined system. This minimum energy is the bandgap of the particle. This is a small but important area of nanotechnology, and the authors would direct the reader to some excellent reviews on the preparation and properties of quantum dots if more detail is required. any nanoparticle will have a very high surface area to volume ratio. The surface area to volume ratio scales with the inverse of the radius. This means that the percentage of atoms available at the surface of a particle for catalysing a reaction will also scale with the inverse of the radius of the particle. For example, a nanoparticle of gold with a diameter of 5 nm will have 31% of its atoms at the surface, whereas at 50 nm this drops to 3.4% and at 1 micron this falls to 0.2%. In addition to the number of surface atoms available for reaction, the chemistry of these sites may also vary from the bulk material because of variations in the lattice structure at the surface of the particle. The result of this is that materials prepared in a nanoparticle form can have much higher activity in catalytic processes than the bulk material and in some cases materials which may be thought of as poor catalysts, such as gold, can be found to have excellent catalytic properties when prepared in a nanoparticle form [12].

3.8 Preparation of nanoparticles

There are two main methods for the preparation of nanoparticles:
top down and bottom up. The former related to the preparation of nanoparticles by ‘‘cutting’’ larger pieces of a material until only a nanoparticle remains. This is commonly achieved using lithographic techniques or etching; however, grinding in

a ball mill can also be used in some cases. The more convenient method for producing nanoparticles
on a commercial scale is to use a bottom-up approach where a nanoparticle is ‘‘grown’’ from simple

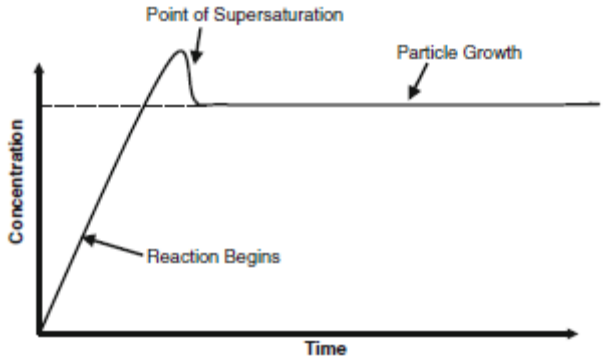

Figure 3.3 A diagram showing a simplified summary of nanoparticle particle formation

molecules. The size of the nanoparticle may be controlled in a number of ways such as limiting the concentration, functionalizing the surface of the particle or using a micelle to template the growth. The bottom-up approach relies on the principle of super saturation to control particle size (Fig. 3.3).

In the early stages of the reaction the concentration of the final material rises rapidly, but no precipitation occurs until the saturation limit is reached (shown by the dotted line). If the reaction is proceeding fast enough the saturation limit may be exceeded before material begins to precipitate from solution. These initial particles will then act as seeds for the final particles and, in an ideal system, any further production of the final material will occur at the particle surface resulting in particle growth. This explanation is very simple and the reality may be much more complex, but this principle is a defining factor in all bottom -up approaches. The

general differences come from the medium in which the reaction is conducted, and this can play a key role in defining the final properties and surface chemistry of the particle. There is insufficient space here to consider all the permutations; however we will discuss some of the common methods employed in preparing the major classes of Nanomaterial's[12].

3.9 Metal oxides

Two methods are commonly used to prepare oxide-based nanomaterials: stabilized precipitation and flame pyrolysis. We will discuss the case for titanium (TiO_2). TiO_2 pigments are commonly prepared by the hydrolysis of titanium sulfate via the sulfate process or by the aerial oxidation of titanium tetrachloride. Similar methods have been used to prepare titanium nanoparticles including the hydrolysis of compounds such as titanium alkoxides in the presence of a capping agent. These methods have the added benefit of further size control and surface functionalization. TiO_2 nanoparticles can also be prepared by oxidizing a solution of titanium tetrachloride ($TiCl_4$) in a flame. Essentially a solution of the metal-oxide precursor is sprayed into a flame, and the oxide particles are formed during the burning process. This method does not allow for any in situ tailored surface functionalization, and any charge stabilization of the final particles will be a result of further reactions upon suspension of the material in a solvent (i.e., water)[13].

3.10 Polymers

Polymer nanoparticles are generally prepared by emulsion polymerisation. In this method an emulsion of monomer (e.g., styrene) is prepared using a non-solvent (i.e., water) and a surfactant (i.e., sodium dodecyl sulfate SDS). The free-radical polymerization is initiated by a water-soluble initiator such as ammonium per sulfate, and the size of the final particles is limited by the dimensions of the micelles. The kinetics of the reaction are so rapid that there are often radicals

trapped in the nanoparticles at the end of polymer chains. The particles formed by this method generally have the surfactant trapped in the polymer particles as their long aliphatic chains either become entangled in the polymer network or as they become grafted onto the polymer by side reactions with the radicals. These particles are therefore usually charge stabilized[13].

3.11 Other particles

There is a wide range of different nanoparticles which have been reported in the literature which are neither polymer nor oxide based. Many of these have been prepared by either stabilized precipitation or by micelle tinplating.

A good example of these is the formation of cadmium sulfide nanoparticles. These particles have been prepared by both methods, which generally rely on the reaction of two precursors such as cadmium chloride and sodium sulfide or the decomposition of a metal organic precursor. Often the surface coating of these particles is hydrophobic, and they do not disperse well in aqueous media; however hydrophilic particles have been prepared. If a micelle method is used to prepare this type of particles, there is no incorporation of the surfactant into the crystal lattice of the final material and therefore it is possible for the surfactant to be removed either by sequential washing or by extreme dilution [13].

3.12 Nanowires and nanotubes

There are several methods for preparing nanowires and tubes, many of which are related to those described above. Currently perhaps the most investigated nanotube is that of carbon (CNT). These nanotubes have not been prepared by simple application of the above methods and require a more complex approach. Usually these materials are prepared by ‘‘growing’’ the tube out of a droplet or

nanoparticle of a metal. In this case a precursor gas such as ethylene is decomposed anaerobically in the presence of a metallic particle. The carbon is rapidly absorbed into the metal droplet and, as the graphitic material begins to form, it migrates to the surface. This eventually results in the extrusion of a wire structure from the surface of the particle. This method is called the vapour-liquid-solid (VLS) method. Clearly the methods used to prepare nanoparticles will have a massive impact on their purity and surface chemistry and therefore also on their final properties. Variations in particle phase, shape, size and surface chemistry can have a massive impact on properties. Similarly, the method of preparation will have an impact on purity, size distribution, surface chemistry and the types of by-products likely to be present in the final material. Understanding these factors is key to understanding the materials we are working with and therefore interpreting the results obtained [13].

3.13 Behavior of nanoparticles in the aquatic environment

Attention has been devoted to the toxicology and implications of NPs, while the environmental behavior of engineered nanoparticles has been less studied. To better understand the likely fate and behavior of NPs in aquatic systems, it is essential to understand their interaction with natural water components such as environmental colloids and natural organic matter under a variety of physicochemical conditions such as pH, ionic strength (I) and type and concentration of cations. Little information about these interactions is yet available specifically for the engineered nanoparticles. Thus, the understanding of environmental impact of NPs will significantly benefit from the previous knowledge about environmental colloids. This section therefore gives an overview on the state of the art in the interaction of NPs with natural water components

(colloids, natural organic matter (NOM), contaminants and cations). It is believed that these interactions will be controlled by processes such as the formation of NOM surface coatings on NPs, aggregation, disaggregation, aggregate structure and interaction with micro pollutants, which are summarized in (Fig. 3.4) and discussed below.

3.14 Interaction with pollutants

In natural aquatic systems, sparingly soluble contaminants are predominantly bound to particle surfaces or complexed by, i.e., humic substances. Due to their high surface to mass ratio, natural NPs play an important role in the solid/water partitioning of contaminants. Contaminants can be adsorbed to the surfaces of NPs, absorbed into the NPs, coprecipitated during formation of a natural NP or trapped by aggregation of NPs which had contaminants adsorbed to their surfaces. In general, it is difficult or even impossible to differentiate between these states or processes, and they may be described as sorption processes (not distinguishing between ad- or absorption). CNTs have been used for the sorption of a variety of organic compounds from water such as dioxins, polyaromatic hydrocarbons (PAH), polybrominated diphenyl ether (PBDEs) chlorobenzenes and chlorophenols and pesticides thiamethoxam. Oxidized and hydroxylated CNTs have also been used for the sorption of metals such as copper, nickel, cadmium, lead, silver, zinc, americium(III) and rare earth metals. Fullerenes have been used for the sorption of organic compounds (naphthalene) and for the removal of organometallic compounds. Zero valent iron-oxide NPs have been applied for the remediation of organic contaminants. Nanoporous ceramic sorbents have been used for the immobilization of cationic metals. Sorption of contaminants onto NPs depends on their properties such as composition, size, purity, structure and solution

conditions such as pH and ionic strength. Pure anatase TiO_2 NPs exhibited stronger affinity and higher sorption capacity than materials that were predominantly composed of anatase with additional amounts of rutile. Acid treatment greatly modified the properties of CNTs such as material purity, structure and nature of the surface which made CNTs become morehydrophilic and suitable for sorption of low molecular weight trihalomethane (THM) molecules. Sorption is size dependent; the affinity of Cu_2+ for hematite follows the order 7 nm [25 nm = 88 nm and sorption on 7 nm particles occurs at lower pH values in comparison toparticles with 25 or 88 nm diameter. indicates the uniqueness of the surface reactivity of iron-oxide NPs with decreasing diameter The sorption capacity of lead to TiO2 NPs (20–33 nm) was always higher, on mass basis, than to the bulk material (520 nm).

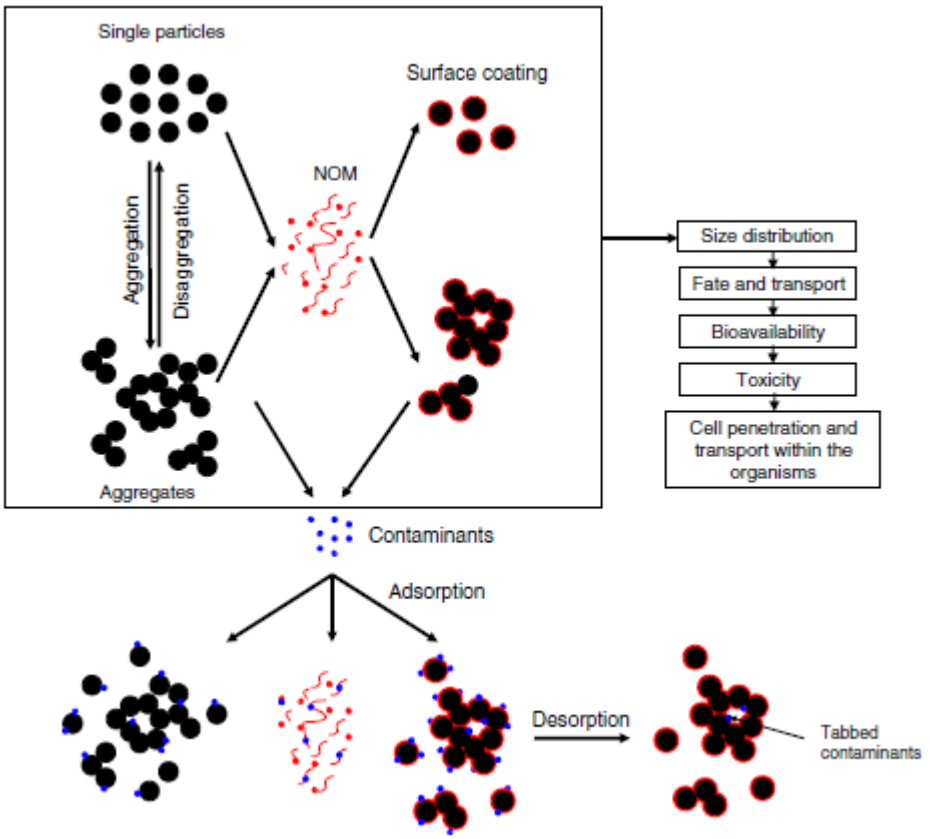

Figure 3.4 Schematic representation of the interaction of engineered NPs with natural water components.

However, the bulk material had a higher sorption capacity when it was normalized to surface area and exhibited stronger affinity. The sorption of contaminants onto C60 fullerenes depends also on aggregate structure (fractal dimension or aggregates porosity, discussed later) and increases by several orders of magnitude with the higher dispersal and porosity of C60. Adsorption/ desorption hysteresis were observed and related to structural Rearrangement of aggregates and the formation of closed interstitial spaces in NP aggregates which prohibit desorption. Porosity increases the time required to reach sorption equilibrium of Zn2+ to

powdered activated carbon (average pore size of 2.46 nm) in comparison with CNT (no pores), as Zn2+ has to move from the exterior surface to the inner surface of the pores. Metals sorption into MWCNTs is pH dependent and shows increasing affinity and capacity with increasing pH as expected from the sorption behavior of metals on to natural colloids carrying a variable surface charge. At pH above the point of zero charge (PZC), surfaces are negatively charged due to the dissociation of surface functional groups providing electrostatic attractions that are favorable for the sorption of cations. The decrease of pH leads to the neutralization or charge reversal of surface charge and so the decrease of caution sorption. The sorption capacity of Zn2+ onto CNT increased with the increase of pH in the pH range (1–8) and reaches a maximum in the range (8–11). The adsorption of trihalomethanes (THM) onto CNTs fluctuates very little in the pH range (3–7), but decreases with pH value as pH exceeds 7. Clearly the interaction of contaminants with NPs is dependent on NPs characteristics such as size, composition, morphology, structure, porosity, aggregation/disaggregation and aggregate structure. However, more research is required to determine and quantify this dependency [13].

3.15 Surface coating by NOM

Previous research on natural colloids has shown that humic substances (HS) form surface films of several nanometers on macroscopic surfaces and on colloidal particles. More recently, it has been shown that HS sorbs to zero-valent iron NPs, iron-oxide NPs, CNT and fullerene NPs, resulting in the formation of nanoscale surface coating. The thickness of this surface coating was found to be of the order of 0.8 nm on iron-oxide NPs in the presence of 25 mg (l-1) humic acid (Baalousha et al. 2008a) and of about 1.0 nm on CNT in the presence of 10 mg l-1 humic acid. The average size of only (0.8–1.0) nm, compared with a known hydrodynamic size

of HA of (1–2) nm, indicates the formation of patchy films or the flattening of the HA molecules on sorption. Such surface coating can modify the nature of NPs. Surface coating has been shown to influence the surface charge of NPs, i.e., suppressing the positive charge and enhancing the negative charge depending on the NP PZC and solution ph. Sorption of HA molecules to iron-oxide NPs, fullerene NPs and CNT was suggested as a stabilization mechanism (enhanced the stability by steric stabilization mechanism) and explained by the increase in electrophoretic mobility. Surface coating of NPs by NOM is likely to affect aggregation behavior (discussed later), resulting in reduced aggregation through charge stabilization and steric stabilization mechanisms (Tipping and Higgins 1982) or enhanced aggregation through charge neutralization and bridging mechanisms caused by fibrillary attachment [13].

3.16 Aggregation of nanoparticles: effect of HA and actions

As with natural colloidal particles NPs are expected to be dominated by aggregation. However, studies on the aqueous stability and aggregation of NPs at environmentally relevant conditions are scant. Brant et al. (2005) studied the aggregation and deposition of fullerene NPs in aqueous media at variable ionic strength. While in the absence of electrolytes C60 stayed stable over time, 0.001 M solution ionic strength (NaCl) was enough to destabilize the C60 by screening their electrostatic charge and produce large aggregates that settle over time. The addition of humic acid has been shown to enhance the stability of fullerene NP suspension in the presence of NaCl and $MgCI_2$ and low concentrations of $CaCI_2$. However, at high Concentrations (above 10 mM) of $CaCI_2$, enhanced aggregation of fullerene NPs was observed due to a bridging mechanism by humic acid aggregates. HA molecules were found to form aggregates, through inter molecular

bridging via calcium complexation, which bridge the fullerene primary particles and enhance their aggregation. This aggregation mechanism has also been observed in the case of alginate-coated NPs undergoing enhanced aggregation through alginate gel formation and in the case of naturally occurring sub-micrometer iron-oxide particles in the presence of NOM and $CaCL_2$ concentrations higher than 10 mM due to a bridging mechanism (Tipping and Ohnstad 1984). Extracted Suwannee River humic acid (SRHA) and natural surface water (actual Suwannee river water with unaltered NOM background) have been shown to stabilize multi-wall carbon nanotubes (MWCNT). The enhancement of the single-walled carbon nanotube (SWCNT) stability in the presence of SRHA, due to nanoscale surface coating and thus increased electrostatic repulsion, was confirmed by. However, extensive flocculation of CNT (i.e., formation of floating aggregates and partial sedimentation of other aggregates of CNT) was observed when mixed with natural waters from a lake, presumably due to the high ionic strength and the presence of divalent cations such as Ca. Apparently, sorption of humic substances enhances the stability and inhibits the aggregation of CNT to a certain extent (Hyung et al. 2007), However, cations, particularly divalent cations such as Ca^{+2} and Mg^{+2}, reduce the stability of CNT in the absence or presence of NOM surface coating. Electrolytes such as NaCI, $MgCl_2$ and $CaCI_2$ induce the aggregation of alginate coated hematite NPs. In the presence of NaCI and $MgCI_2$, alginate-coated hematite nanoparticles aggregate through electrostatic destabilization. In the presence of $CaCI_2$, the aggregation rate was much higher than that which conventional diffusive aggregation predicts. This was explained by the formation of an alginate-coated hematite gel network and the crosslinking between unadsorbed alginate that might form bridges between hematite-alginate gel structures. The increase of solution pH was found to induce the aggregation of

iron-oxide NPs with maximum aggregation close to the point of zero charge (PZC) of about 8.0. The addition of SRHA was found to shift the PZC and the aggregation of iron-oxide NPs to lower pH values, neutralize the positive surface charge at pH values below the PZC and to enhance the negative charge at pH values above the PZC. Thus, in this case SRHA had a dualrole as a coagulant or a stabilizer below and above the PZC, respectively. Other than pH, ionic strength and NOM, the concentration of NPs can influence their aggregation behavior. Concentration-dependent aggregation of iron-oxide NPs and zero-Valente iron oxide has been observed. The rate of aggregation and size of individual aggregates formed increased with increasing particle concentration. Obviously, natural waters will have complex effects on NP stability, aggregation and sedimentation through different mechanisms of Nano scale surface film formation, charge enhancement and steric stabilization by NOM, charge neutralization by ionic strength or specifically by binding cations such as Ca, bridging by fibrils and bridging by aggregated NOM. These interactions need further investigation in order to predict the fate and behavior of engineered NPs in natural aquatic system[13].

3.17 Variation in aggregates structure in function of HA concentration: fractal dimension

The conformation and porosity of NP aggregates vary significantly with the medium physicochemical conditions such as pH, ionic strength, concentration of NPs and concentration of NOM. The structure of NP aggregates can be described by fractal dimension. Fractal dimension provides information about the morphology of the aggregate related to the irregularity, the mass distribution within the aggregate, aggregate porosity and compactness. Fractal dimension has a value in the range (1–3): 1 for a linear aggregate and 3 for a compact sphere. Aggregates of NPs such as fullerenes, CNT, iron oxide, and natural colloidal

particles have been observed to form fractal structures. The fractal dimension of kaolin aggregates decreased with the addition of HA to a minimum value and stayed constant with the further increase of HA. The fractal dimension of iron-oxide NPs was found to vary in the presence of HA molecules. For instance, (Fig. 5), a typical TEM micrograph, shows the variation of aggregate structure due to the addition of SRHA molecules at PH 6. In the absence of HA, iron-oxide NPs form open porous aggregates with a fractal dimension (D_1 1.16 ± 0.06), (D_2 1.78 ± 0.06) and (D_3 1.87 ± 0.06), whereas in the presence of HA, they form compact aggregates with a fractal dimension (D_1 1.74 ± 0.10), (D_2 1.95 ± 0.01) and (D_3 2.06 ± 0.02). Aggregate structure is an important factor, controlling their fate and behavior and their interaction with contaminants.

The more porous the aggregate, the lower the fractal dimension, resulting in faster sedimentation in comparison to higher fractal aggregates or impermeable spheres. Adsorption/desorption hysteresis of naphthalene to fullerenes NPs was explained by the blockage of the pores with the aggregates after sorption takes place, i.e., variation in their fractal dimension. Aggregate structure also influences their disaggregation as will be discussed later [13].

3.18 Disaggregation of NPs by HA molecules

Disaggregation is as important as aggregation processes in determining NPs fate and behavior and interaction with trace contaminants. However, no studies are available on the disaggregation of NPs except one study performed on iron-oxide NPs. NOM has been shown to induce the disaggregation of iron-oxide NP aggregates (5–10) nm, likely due to formation of surface coating of NOM on the surface and pore surface of the aggregates and thus the enhancement of surface charge as confirmed by electrophoretic mobility measurements. This induces an increase of the degree of repulsion within the aggregate matrix and results in

aggregate rupture. A previous study has shown that polymers are able to separate two stuck colloids, even when the separation distance was on the order of few nanometers (primary minimum). There are two possible mechanisms of aggregate breakup based on aggregates structure, i.e., the location of the weakest cross section where the aggregates might break and given the different rates of disaggregation: surface erosion (slow rate) and large-scale fragmentation. In surface erosion, small particles are separated from the surface

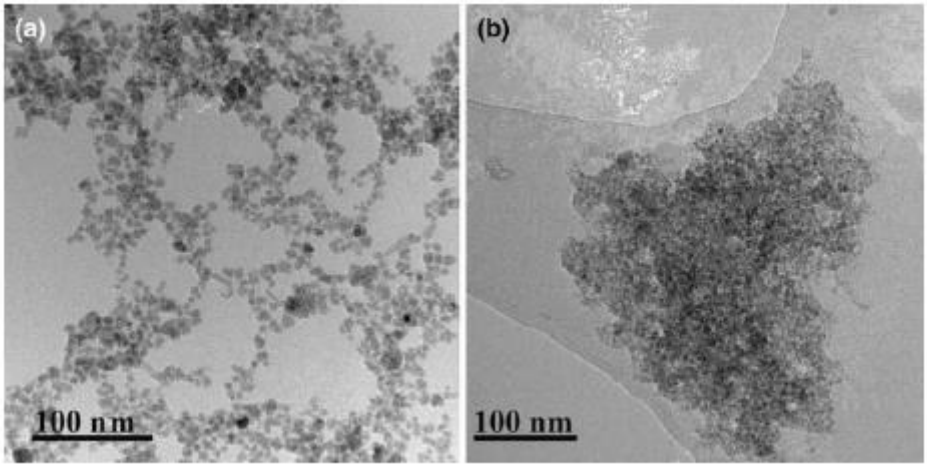

Figure 3.5 Variation in the structure of iron-oxide nanoparticles due to the interaction with SRHA molecules at PH 6 as observed by transmission electron microscope (a) FeO (100 mg l-1 Fe) and (b) FeO (100 mg l-1 Fe) + HA (5 mg l-1), scale bar = 100 n. of the aggregate while in large-scale fragmentation (fast rate) the aggregates split into pieces of comparable sizes. Highly branched aggregates with small fractal dimension breakup by fragmentation mechanisms, while compact aggregates with high fractal dimension favour breakup by surface erosion mechanisms. Disaggregation depends also on the way NP aggregates interact with HA. HA adsorption on NP aggregate surfaces may develop in two steps. The first, fast step corresponds to purely covering the aggregate apparent surface by HA and a second slower step corresponds to the diffusion of HA through the already

adsorbed layer and the reputation of HA into the restricted zones near to neighboring interfaces, i.e., aggregate pores. It has been shown that the adsorption of polyelectrolyte to colloidal particles surfaces induced aggregate fragmentation after an initial lag time, which is the time required for polymer reptation within the porous matrix of aggregates and sorption to the surface of the particles. Clearly the disaggregation depends on the structure of the aggregates, i.e., their fractal dimension, and more research is needed to investigate the possible disaggregation of NPs in the environment and the role of natural organic matter on this process.

3.19 Environmental significance

NPs may impact the environment in three possible ways:

(1) direct effect on biota, i.e., toxicity,

(2) changes in the bioavailability of toxins or nutrients,

(3) indirect effects on ecosystem, i.e., break-up of refractory natural organic substances and

(4) changes of the environmental microstructures.

Understanding the interactions between NPs and natural colloids is crucial to estimate the potential impact of NP and ensure environmentally sustainable production and use of NPs. This review shows that the exact behavior will depend in a complex manner on NP properties, organic matter type and concentration and on solution conditions such as pH and ionic strength. Surface coating, aggregation and disaggregation will largely determine the bioavailability and the fate and behavior of NPs through (1) controls on transport in surface and ground waters and (2) sedimentation in surface waters or deposition and filtration in soils and groundwater's. Stabilization of NPs by surface coating may maintain them within the water column and increase their transportation distances and rates. Aggregation will likely lead to settling of NPs to the sediments and consequently to reduced

transportation in the water column, which potentially makes benthic organisms a key receptor for NPs. Disaggregation will result in the formation of small aggregates that can be resuspended and become mobile in the water column and which may carry pollutants as well as nutrients, and thus results in their transport (Fig. 3.6). Aggregation and sedimentation of NPs can be responsible for the scavenging of colloids from the water column to the sediment and will lead to the formation of porous microstructures of both natural colloids and NPs that can change their structure (fractal dimension) depending on the medium physicochemical conditions, i.e., pH, ionic strength, concentration of NPs and concentration of NOM. The porosity of these microstructures/ aggregates controls the circulation of water, nutrients and soluble compounds within the aggregates, sorption of chemicals and sedimentation rate. Each of the components of microstructures (i.e., NPs, colloids and NOM) can adsorb significant amounts of nutrients and thus serve as nutrient reservoirs for the microorganisms

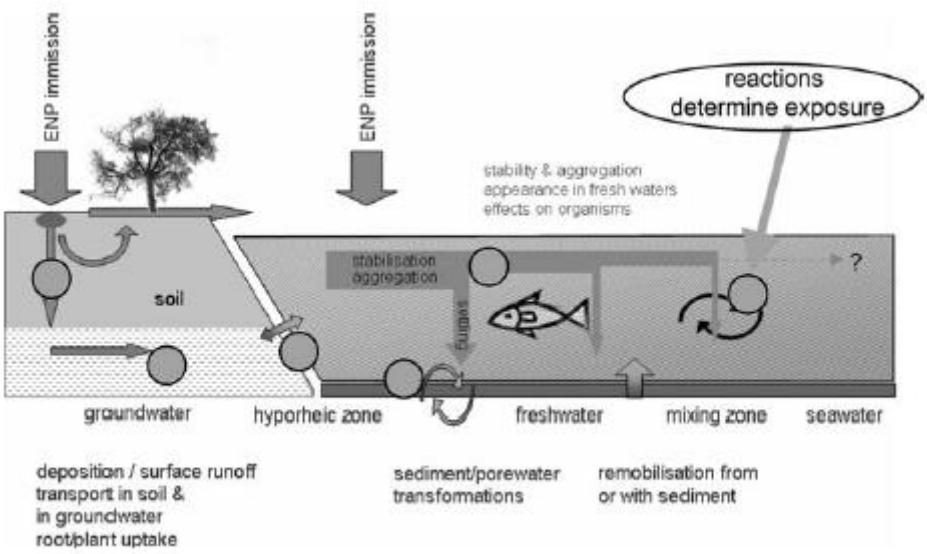

Figure (3.6) Schematic plot of pathways and important transformation reactions in the aquatic environment.

that are included within the microstructure. Therefore, the introduction of NPs into aquatic medium will influence its microstructure, metals and nutrient bioavailability and ultimately the sustainability of life [13].

3.20 Behavior in porous media General mechanism

The transport of NPs in porous media is, among others, dominated by their size, shape and charge distribution. Transport or filtration of NPs in porous media like soils or aquifers is divided into two steps: (1) collision and (2) attachment to the soil or sediment grains themselves (the collector). While the attachment is a function of the electrostatic interactions between the NPs and the soil, the mechanisms leading to a collision can be further divided into surface, straining and physical–chemical filtration. If NPs are prevented from penetrating into the media due to their size, a filter cake or a surface mat will form above the media (surface filtration). NPs which are capable of entering the media can be mechanically removed by sieving or straining in smaller pore spaces (straining filtration/sieving). In addition, for unsaturated systems, filtration at a gas-water interface has to be taken into account. For small NPs physical and chemical forces are decisive. The collisions of small NPs with a collector occur as a result of three processes: diffusion, interception and sedimentation Fig. (3.7).

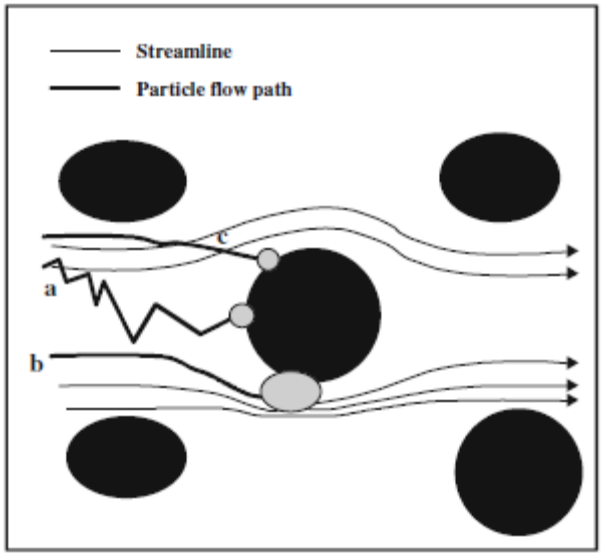

Figure 3.7 Particle filtration by (a) diffusion, (b) interception and (c) sedimentation (modified after Yao (1968))

Small NPs and aggregates (\1 lm) are mainly transported by Brownian diffusion. NPs which move on their flow path close to the soil material can make contact by interception. This is attributed to a difference of NP velocity and collector. A further agglomeration mechanism takes place due to differences in density. For NPs with a higher density than the transport medium the sedimentation process has to be considered. Finally, (not displayed in Fig. 3.3), NPs can be retained in the soil by pore size exclusion or sieving. While the maximum size of mobile NPs is limited by straining filtration and pore velocity, concentration and size distribution of NPs in the nanometer size range are controlled by physico-chemical filtration. A minimum filtration rate can be observed at a size range close to 1 lm for a density close to 1 g/cm3 and around 0.2 lm for NPs with a density around 3 g/cm3, where straining filtration is less effective in most systems and physico-chemical filtration does not yet reach its maximum [13].

3.21 Filtration models for NPs/porous media collision

Iwasaki (1937) described filtration as a first order kinetic,

$$C_P = C_{0P} e^{(-\lambda \cdot \Delta x)} \quad (1)$$

And

$$R_T = -\frac{1}{\lambda} \ln\left(\frac{C_P}{C_{0P}}\right) \quad (2)$$

where CP is the NP concentration at the travel distance x, C0P is the original NP concentration, k is the filtration factor in m-1 and RT is the colloid travel distance in m at a given retention rate. The correlation between the filtration factor and travel distance is given in Fig. 10. Developed by Yao (1968), Yao et al. (1971) and extended by Rajagopalan and Tien (1976), the so-called filtration theory enabled the calculation of the filtration.

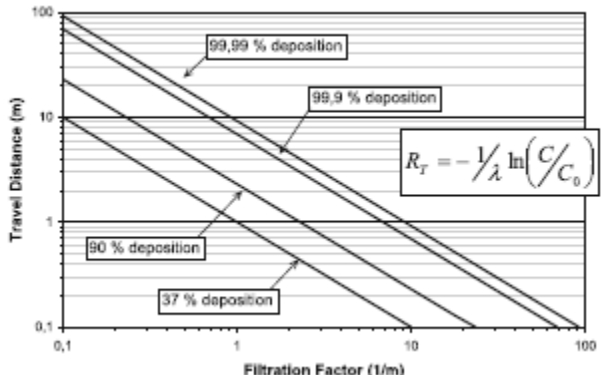

Figure (3.8) Correlation between filtration factor and travel distance for a given deposition rate

Chapter four

Material and Methods

4.1 Introduction

Sample of Nano sized silicon was prepared in order to study optical properties

4.2 Instruments

XRD Devices-Different sample of silicon

A **B**

Figure (4.1) X-Ray diffraction device(XRD device).

4.3 Material

A sample of silicon dioxide was brought and crushed, then scraped and then grinded in three stages. The first phase was grinding for a minute, a sample of silicon dioxide was brought and crushed, then scraped and then grinded in three stages. The first phase was grinding for a minute, the second stage was grinding for two minutes, the third stage was milling for three minutes, then the two eyes were placed in the x-ray diffraction apparatus to study optical properties.

4.4 The Method

Using X R D devices which available Criminal Evidence, the optical properties were tabulated in table (4.1) and the graph (4.1) of transmission versus angle of diffraction was drown.

4.5 Result

The results obtained was graphed in the figure below.

Table (4.1) shows the relation between intensity and angle (2Ɵ) for sample one (crushed for one minute)

β^o	Intensity	Transmission (T)	Absorption (A)
10	150	1	0
15	119	0.79	0.21
20	80	0.53	0.47
25	50	0.33	0.67
30	99	0.66	0.34

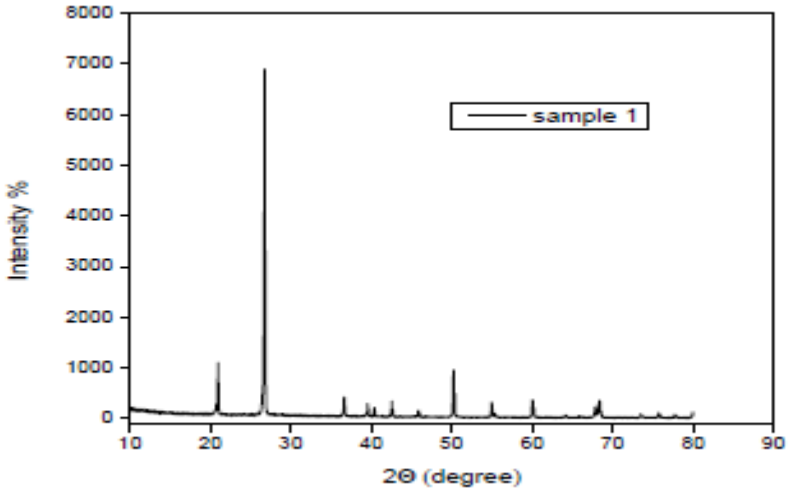

Figure (4.2) shows the relation between intensity and diffraction angle (2Ɵ) for sample one (crushed for one minute)

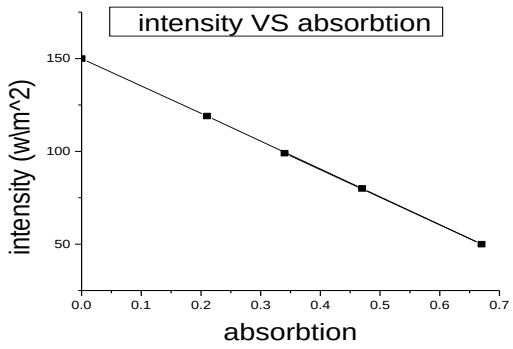

Figure (4.3) shows the relation between intensity Absorption for sample one (crushed for one minute)

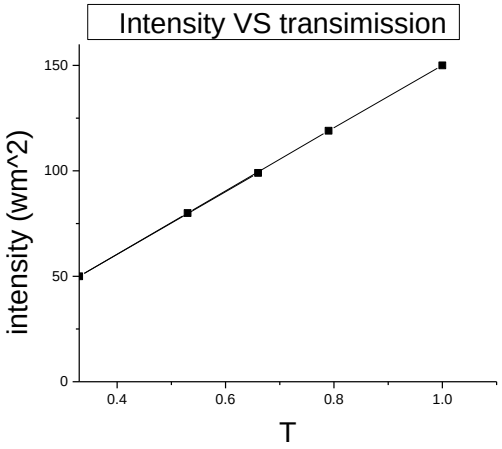

Figure (4.4) shows the relation between intensity Transmission for sample one (crushed for one minute)

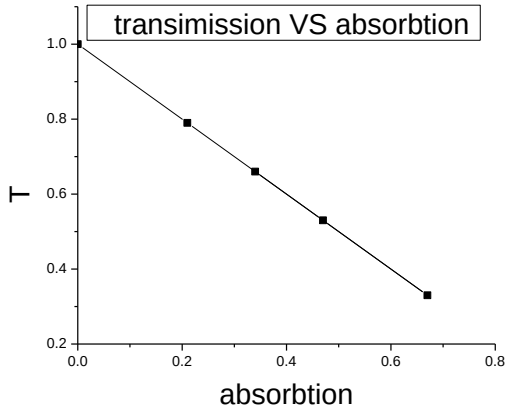

Figure (4.5) shows the relation between Transmission and Absorption for sample one (crushed for one minute)

Table (4.2) shows the relation between intensity and angle (2Ɵ) for sample one (crushed for two minute)

β^o	Intensity	T	A
30	150	1	0
35	58	0.38	0.62
40	55	0.36	0.64
45	37	0.24	0.76
50	51	0.34	0.66

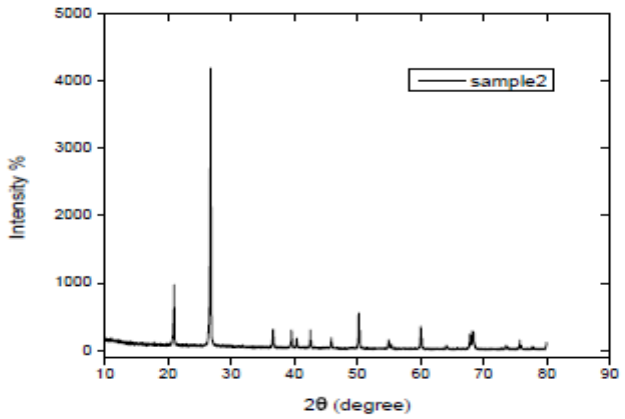

Figure (4.6) shows the relation between intensity and diffraction angle (2Ɵ) for sample two (crushed for two minute)

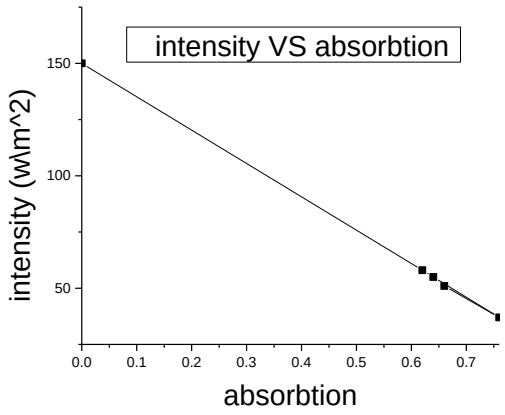

Figure (4.7) shows the relation between intensity and Absorption for sample two (crushed for two minute)

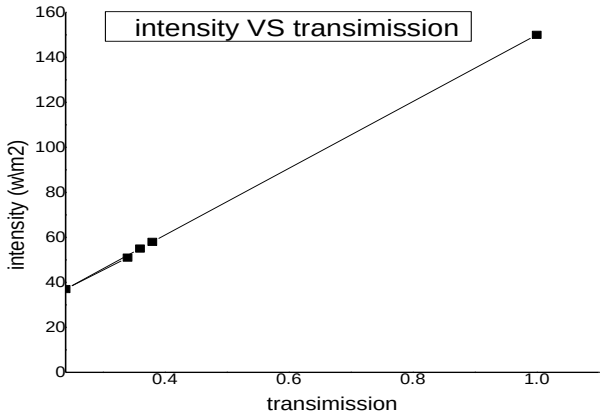

Figure (4.8) shows the relation between intensity and Transmission for sample two (crushed for two minute)

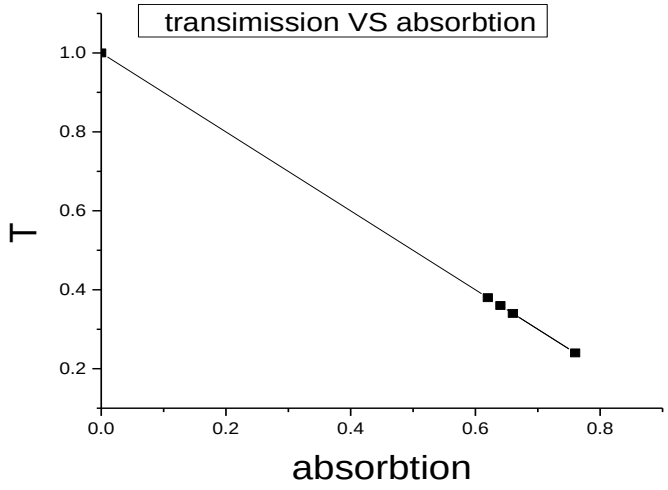

Figure (4.9) shows the relation between Transmission and Absorption for sample two (crushed for two minute)

Table (4.3) shows the relation between intensity and angle (2Ɵ) and transmission and abortion for sample three (crushed for three minute)

β^o	Intensity	T	A
55	150	1	0
60	77	0.51	0.49
65	59	0.39	0.61
70	28	0.18	0.82
75	16	0.11	0.89

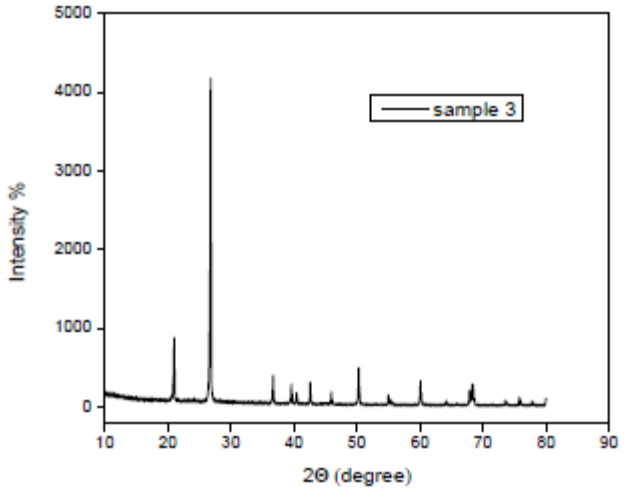

Figure (4.10) shows the relation between intensity and diffraction angle (2Ɵ) for sample three (crushed for three minute)

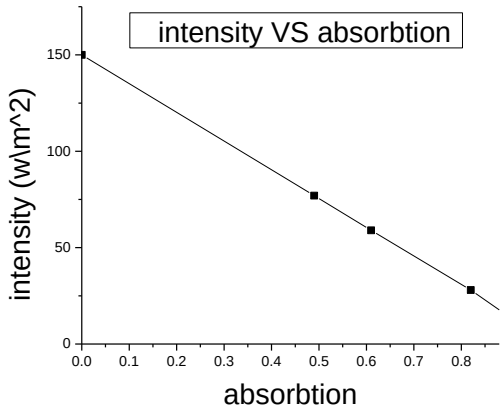

Figure (4.11) shows the relation between intensity and Absorption for sample three (crushed for three minute)

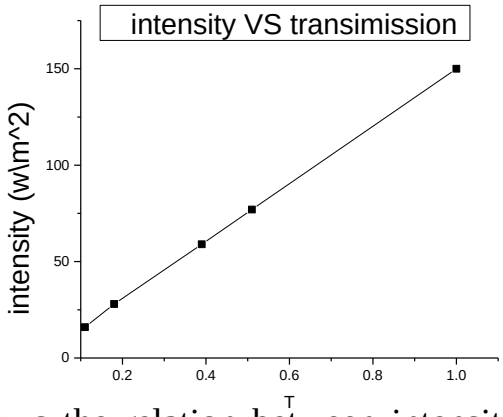

Figure (4.12) shows the relation between intensity and Transmission for sample three (crushed for three minute)

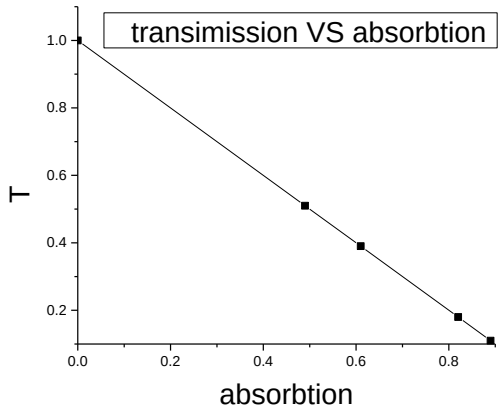

Figure (4.12) shows the relation between Transmission and Absorption for sample three (crushed for three minute)

Table (4.4) shows the relation between intensity and angle (2Ɵ) and transmission and absorption for all sample.

β^o	Intensity	T	A
10	150	1	0
15	119	0.79	0.21
20	80	0.53	0.47
25	50	0.33	0.67
30	99	0.66	0.34
30	150	1	0
35	58	0.38	0.62
40	55	0.36	0.64
45	37	0.24	0.76
50	51	0.34	0.66
55	150	1	0
60	77	0.51	0.49
65	59	0.39	0.61
70	28	0.18	0.82
75	16	0.11	0.89

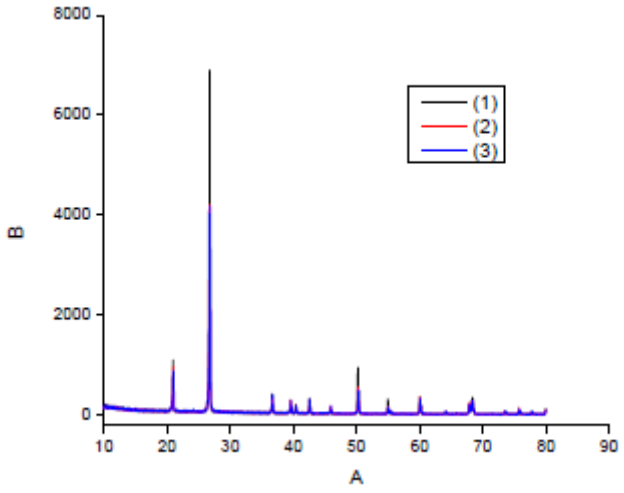

Figure (4.13) shows the relation between intensity and diffraction angle (2Ɵ) for all samples.

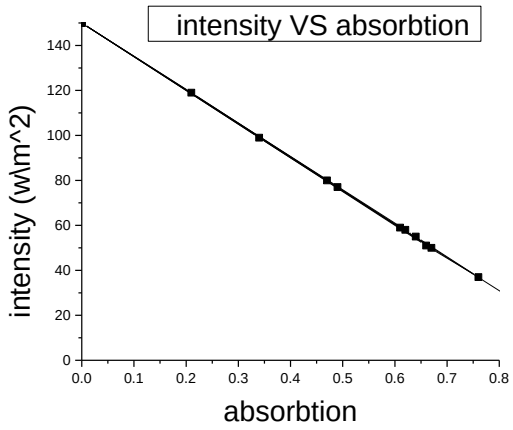

Figure (4.14) shows the relation between intensity and Absorption for all samples.

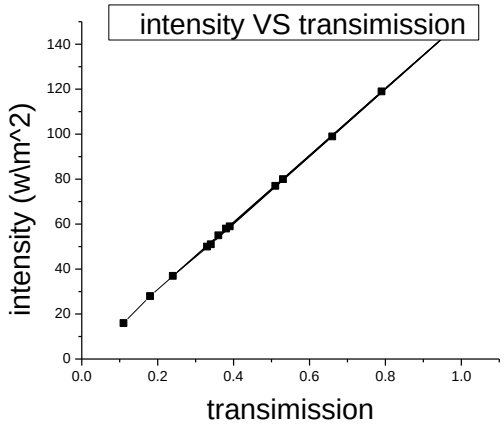

Figure (4.15) shows the relation between intensity and Transmission for all samples.

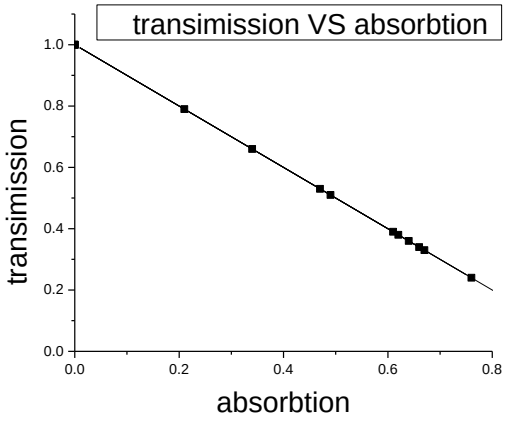

Figure (4.16) shows the relation between Transmission and Absorption for all samples.

$$A' = -\ln\left(\frac{I}{I_0}\right) \tag{4.1}$$

$$A = \varepsilon \ell c = \alpha \ell \tag{4.2}$$

And

$$A' = \sigma \ell N = \alpha' \ell \tag{4.3}$$

The amount of photons absorbed in the chip is then given as follows:

$$\frac{dI_z}{I_z} = -\sigma N \, dz. \tag{4.4}$$

The solution of this simple differential equation can be obtained by combining the two sides to obtain I_Z as a character of Z:

$$\ln(I_z) = -\sigma N z + C. \tag{4.5}$$

The difference in intensity in the slide for true thickness ℓ is I_0 at z = 0, and I_1 at z = ℓ. Using the previous equation, write the difference in severity as follows:

$$\ln(I_0) - \ln(I_\ell) = (-\sigma 0 N + C) - (-\sigma \ell N + C) = \sigma \ell N \tag{4.6}$$

By rearranging the equation, it becomes as follows:

$$T = \frac{I_1}{I_0} = e^{-\sigma \ell N} = e^{-\alpha' \ell}. \tag{4.7}$$

This means that:

$$A' = -\ln\left(\frac{I_1}{I_0}\right) = \alpha' \ell = \sigma \ell N \tag{4.8}$$

$$A = -\log_{10}\left(\frac{I_1}{I_0}\right) = \frac{\alpha' \ell}{2.30} = \alpha \ell = \varepsilon \ell c \tag{4.9}$$

In practice, the accuracy of the hypothesis is better than the accuracy of most spectroscopic measurements until the absorption value is equal to 1

Or:

$$I_1 / I_0 = 0.1 \tag{4.10}$$

At a good approximation, absorptive polysaccharides in this field have a linear relationship with the concentration of sorbents in the solution. At large absorption values, the estimated concentration value will decrease due to the effect of blocking molecules unless non-linearity is applied between absorption and concentration.

4.6 Discussion

From the figures (4.3), (4.7), (4.11) and (4.14), which shows the relationship between intensity and absorption, found that the greater the intensity less absorption.

From the figures (4.4), (4.8), (4.12) and (4.15), which shows the relationship between intensity and transmission, found that the higher the intensity of the increased transmission. From Figures (4.5), (4.9), (4.13) and (4.16), this shows the relationship between absorption and transmission, proved the inverse relation between them.

4.7 Conclusion

Absorption decreases with increased intensity and increases with decrease. The transition increases with increasing intensity. The inverse correlation between absorption and transition occurs.

4.8 Recommendation

- Use different samples of silicon dioxide in Nano scale size and study their properties after grinding at different times.
- Use a simulation program to find sample thickness in Nano scale size to calculate the attenuation coefficient.

4.9 References

[1] Batista, Carlos A. Silvera; Larson, Ronald G.; Kotov, Nicholas A. (2015-10-09). "Nonadditivity of nanoparticle interactions". Science. 350 (6257): 1242477. doi:10.1126/science.1242477. ISSN 0036-8075. PMID 26450215.

[2] Bibo Li, Dapeng Yu, and Shu-Lin Zhang Raman Vol. 59, Iss. 3 — 15 January 1999.

[3] Taylor, Robert A.; Otanicar, Todd P.; Herukerrupu, Yasitha; Bremond, Fabienne; Rosengarten, Gary; Hawkes, Evatt R.; Jiang, Xuchuan; Coulombe, Sylvain (2013).

[4] CPWR-Center for Construction Research and Training — Work Safely with Silica.

[5] Hornung, Veit; Bauernfeind, Franz; Halle, Annett; et al. (2008). "Silica crystals and aluminum salts activate the NALP3 inflammasome through phagosomal.

[6] Wikipedia

[7] Module 3: Characteristics of Particles – Particle Size Categories. epa.gov

[8] Taylor, Robert A; Otanicar, Todd; Rosengarten, Gary (2012). "Nanofluid-based optical filter optimization for PV/T systems". Light: Science & Applications

[9] Hewakuruppu, Y. L.; Dombrovsky, L. A.; Chen, C.; Timchenko, V.; Jiang, X.; Baek, S.; Taylor, R. A. (2013). "Plasmonic "pump–probe" method to study semi-transparent nanofluids". Applied Optics.

[10] Taylor, Robert A.; Otanicar, Todd P.; Herukerrupu, Yasitha; Bremond, Fabienne; Rosengarten, Gary; Hawkes, Evatt R.; Jiang, Xuchuan; Coulombe, Sylvain (2013).

[11] Rondeau, V.; Jacqmin-Gadda, H.; Commenges, D.; Helmer, C.; Dartigues, J.-F. (2008). "Aluminum and Silica in Drinking Water and the Risk of Alzheimer's Disease or Cognitive Decline

[12] Kittel, Volume 568, Issues 1–2, 24 May 2006, Pages 28-40.

[13] Journal of Physics C: Solid State Physics, Volume 17, Number 35.